Accepted Manuscript

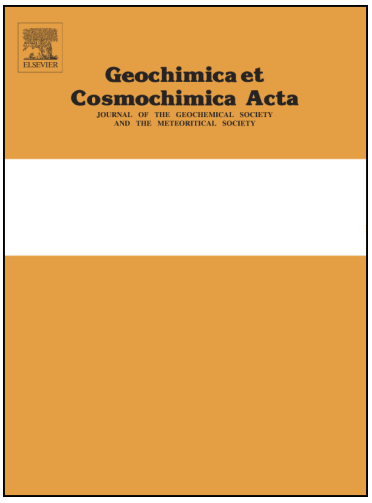

Modeling the carbon isotope signatures of methane and dissolved inorganic carbon to unravel mineralization pathways in boreal lake sediments

F. Clayer, A. Moritz, Y. Gélinas, A. Tessier, C. Gobeil

PII: S0016-7037(18)30082-6
DOI: https://doi.org/10.1016/j.gca.2018.02.012
Reference: GCA 10655

To appear in: *Geochimica et Cosmochimica Acta*

Received Date: 10 February 2017
Accepted Date: 2 February 2018

Please cite this article as: Clayer, F., Moritz, A., Gélinas, Y., Tessier, A., Gobeil, C., Modeling the carbon isotope signatures of methane and dissolved inorganic carbon to unravel mineralization pathways in boreal lake sediments, *Geochimica et Cosmochimica Acta* (2018), doi: https://doi.org/10.1016/j.gca.2018.02.012

Modeling the carbon isotope signatures of methane and dissolved inorganic carbon to unravel mineralization pathways in boreal lake sediments

F. Clayer[a,c], A. Moritz[b,c,1], Y. Gélinas[b,c], A. Tessier[a] and C. Gobeil[a,c]

[a] INRS-ETE, Université du Québec, 490 rue de la Couronne, Québec (QC), Canada G1K 9A9

[b] Department of Chemistry and Biochemistry, Concordia University, 7141 Sherbrooke Street West, Montreal (Qc), Canada H4B 1R6

[c] Geotop Research Center, Montréal, Canada

[1] Present address: ISOSPARK, 2298 chemin Saint-François Dorval (Qc), Canada H9P 1K2

Corresponding author: francois.clayer@ete.inrs.ca; Phone: +1 418 654 3772

Email addresses:

Anja Moritz – anja.moritz@isospark.com

Yves Gélinas – yves.gelinas@concordia.ca

André Tessier – andre.tessier@ete.inrs.ca

Charles Gobeil – charles.gobeil@ete.inrs.ca

Abstract

Vertical profiles of the concentration and isotopic composition ($\delta^{13}C$) of methane (CH_4) and dissolved inorganic carbon (DIC), as well as of ancillary parameters, were obtained in the top 25 cm sediment column of a seasonally anoxic basin from an oligotrophic boreal lake. Modeling the profiles of CH_4 and DIC concentrations and those of their $\delta^{13}C$ signatures with reaction-transport equations allowed us to determine the organic matter (OM) degradation rates according to various reactions and to constrain the *in situ* isotopic fractionation factors and diffusivity coefficients of CH_4 and DIC. This exercise reveals *inter alia* that (i) CH_4 production occurs below 5 cm depth, with the highest production rate between 5 and 7.5 cm depth, (ii) all CH_4 is produced through hydrogenotrophy, and (iii) methanogenesis yields a production rate of CH_4 about three times greater than that of DIC. This latter observation indicates either that fermentation of OM is not the exclusive source of H_2 sustaining hydrogenotrophy, or that the commonly assumed model molecule CH_2O does not adequately represent the fermenting OM, since its fermentation yields identical rates of CH_4 and DIC production. The porewater profiles of Fe and SO_4^{2-} suggest that some H_2 may be produced during the reoxidation of reduced sulfur by Fe(III), but the rate of H_2 production via this process, if active, would be insignificant in comparison to that required to sustain the estimated rate of hydrogenotrophy. We deduce that the imbalance between CH_4 and DIC production rates is rather due to the fermentation of organic substrates that are more reduced than CH_2O, i.e., having a negative average carbon oxidation state (COS). From the constraints on reaction rates and on fermentation pathways imposed by the $\delta^{13}C$ data, we infer that the organic substrate fermenting between 5 and 7.5 cm depth should have a COS of −1.87.

We thus submit that CH_4 is produced in the sediments of the seasonally anoxic basin of our boreal lake through hydrogenotrophy coupled to the fermentation of reduced organic substrates that can be represented by a mixture of fatty acids (e.g. $C_{16}H_{32}O_2$; COS of −1.75) and fatty alcohols (e.g., $C_{16}H_{34}O$; COS of −2.00). This study emphasizes the importance of characterizing the sedimentary OM undergoing mineralization in order to improve diagenetic model predictions of CH_4 cycling in boreal lakes and of its significance in climate change.

Keywords

Methane, organic matter mineralization, reaction-transport modeling, carbon isotopes, boreal lake, sediment porewater, early diagenesis

1. INTRODUCTION

Aquatic sediments represent a key medium through which organic carbon (C_{org}) originating mainly from the photosynthetic activity in the biosphere (Arndt et al., 2013) is transferred to the geosphere (Tissot and Welte, 1984). During its burial in sediments, C_{org} undergoes a complex suite of degradation reactions that yield various intermediate compounds and two greenhouse gases: carbon dioxide (CO_2) and methane (CH_4). Microbially-mediated processes produce (methanogenesis) and consume (methanotrophy) CH_4 in sediments, and these opposite processes control the CH_4 flux from the sediments to the water column and eventually to the atmosphere. Although CH_4 is emitted at a lower rate and has a shorter lifetime in the atmosphere than CO_2, its radiative impact is up to 105 times greater on a 20-year horizon (Shindell et al., 2009).

After a short period of stabilization in the early 2000's, CH_4 global emissions rose again in the last decade at an unexpected high rate (Nisbet et al., 2014) only predicted by the worst case scenario of the Intergovernmental Panel on Climate Change (IPCC, 2013). Since large uncertainties in the global CH_4 budget arise from the ill-known CH_4 emissions from continental waterbodies to the atmosphere (Saunois et al., 2016), it is important to clarify the pathways of methanogenesis and their importance relative to other C_{org} mineralization pathways, including methanotrophy and C_{org} fermentation, in freshwater sediments. Quantifying these processes is intricate because it involves numerous reactions, organic compounds, microorganisms and oxidants, as well as several transport processes (Berner, 1980). Reaction-transport models have the potential to capture this complexity and can thus act as powerful tools for interpreting present-day observations and for predicting how C_{org} degradation processes are altered under transient

environmental scenarios (Paraska et al., 2014). The successful application of this modeling approach requires, however, an adequate formulation of the chemical composition of the metabolizable C_{org} and of the reactions involved in its respiration.

Natural organic matter (OM) deposited at the sediment surface is an intricate mixture of biopolymers such as cellulose, lignin, proteins, lipids, humic substances (HS) and carbohydrates (Hedges and Oades, 1997; Burdige, 2006). In modeling OM oxidation and fermentation, it is commonly assumed that the bulk metabolizable OM can be represented by CH_2O (Arning et al., 2016), which is a simplification for several compounds (e.g., carbohydrates, cellulose) whose average carbon oxidation state (COS) is zero. This approach has mainly been applied to marine settings (Arndt et al., 2013; Paraska et al., 2014; Arning et al., 2016 and references therein), where OM is essentially derived from algae. The general applicability of CH_2O as a representation of metabolizable OM can nevertheless be questioned. For example, the analyses of marine plankton samples from five different sites by nuclear magnetic resonance revealed that the COS of plankton biomass was negative (Hedges et al., 2002). The mineralization of OM that is more reduced than CH_2O was also proposed as a possible explanation for low ratios (< 2) of DIC : SO_4 fluxes observed in coastal and continental margin sediments (Alperin et al., 1994; Berelson et al., 2005; Jørgensen and Parkes, 2010; Burdige and Komada, 2011). Moreover, Clayer et al. (2016) determined by inverse modeling of porewater CH_4 and DIC profiles, that production rates of CH_4 were 2–4 times greater than those of DIC in boreal lake sediments at depths, where only methanogenesis is occurring. This result is incompatible with the fermentation of CH_2O, which would yield

equivalent production rates of CH_4 and DIC, and suggests that the fermenting organic substrates are more reduced than CH_2O.

Understanding the reactions responsible for OM degradation in lake sediments, including those leading to CH_4 production and consumption, is crucial for a number of reasons. For example, there are at least 25 million lakes on Earth, with the greatest abundance in boreal regions (Verpoorter et al., 2014), and it is estimated that lakes globally bury more C_{org} (Tranvik et al., 2009) and release five times more CH_4 to the atmosphere than the world oceans (Bastviken et al., 2004). Furthermore, the large body of knowledge about CH_4 cycling in marine sediments does not necessarily apply to freshwater sediments. Concentrations of OM are often found to be one order of magnitude higher in freshwater than in marine sediments and the geochemical characteristics of the OM strongly differ between these two types of sediments (e.g., Westrich and Berner, 1984; Hedges and Oades, 1997).

In this study, we report centimeter-scale porewater profiles of the concentration and stable carbon isotope ratios of CH_4 and DIC, as well as ancillary data for key geochemical parameters, in sediment cores and porewater samples. Through diagenetic modeling, this extensive dataset is used to quantify the rate of the reactions responsible for OM mineralization and to estimate the COS of the fermenting organic substrates.

2. METHODS

2.1. Sampling

This study was carried out in a 22-m deep basin of Lake Tantaré (47°04'N, 71°32'W), a 1.1-km^2 headwater lake of low primary productivity (~50 mg C m^{-2} d^{-1};

Hare et al., 1994) located near Quebec City in a fully forested and uninhabited ecological reserve sited at the southern limit of the Canadian Shield. The bottom water of this circumneutral and oligotrophic basin becomes occasionally anoxic at the end of the summer (Couture et al., 2008). The C_{org} concentration remains relatively constant over the top 30-cm of the sediment column (20 ± 2%; Clayer et al., 2016) and the elevated sediment C_{org} : N molar ratio (17 ± 2; Clayer et al., 2016) and the $\delta^{13}C_{org}$ values (−28‰ to −29‰; Joshani, 2015) indicate that particulate OM is dominated by terrestrial HS.

Sediment porewater was collected in October 2014, when bottom water O_2 concentration was < 0.1 mg L^{-1}, by in situ dialysis with peepers (Hesslein, 1976; Carignan et al., 1985) deployed by divers within an area of about 25 m² at the deepest site of the basin. The peepers were acrylic devices comprising two columns of 4-mL cells filled with ultrapure water, covered by a 0.2-µm Gelman HT-200 polysulfone membrane and allowing porewater sampling at a vertical resolution of 1 cm from about 23 cm below the sediment-water interface (SWI) to 5 cm above this interface (thereafter referred to as overlying water). Removal of dissolved oxygen from the peepers prior to their deployment was done as described by Laforte et al. (2005). Three peepers with pre-drawn horizontal lines were inserted into the sediment and left in place for 21 d, i.e., a longer time period than that required (5–10 d) to reach equilibrium between porewater and the water in the peeper cells for various solutes (Hesslein, 1976; Carignan et al., 1985), including CH_4 and dissolved inorganic carbon (DIC). The peepers with a pre-drawn horizontal line were inserted slowly into the sediments until the horizontal line just disappeared from view, which defined the SWI. This number of peepers was required to determine three independent profiles of pH and of the concentrations of CH_4, DIC,

acetate, NO_3^- and SO_4^{2-}, as well as duplicate profiles of dissolved sulfide (ΣS(−II)), Fe and Mn.

Samples (~ 1 mL) for CH_4 and DIC were collected within 5 minutes from peeper retrieval with He-purged polypropylene syringes and injected through rubber septa into He-purged 3.85-mL exetainer vials (Labco Limited) preacidified with 40 µL of HCl 1N to reach a final pH ≤ 2 and convert all DIC into CO_2. A volume of ~ 1 mL of He was removed from each exetainer vials prior to sample injection to avoid overpressure. The protocols used to collect and preserve water samples for the other solutes are described by Laforte et al. (2005).

2.2. Analyses

Porewater concentrations of CH_4 and total CO_2 were measured within 24 h of peeper retrieval with a gas chromatograph (GC; Perkin Elmer Sigma 300) equipped with a Porapak-Q column, a methanizer and a flame ionization detector as described by Clayer et al. (2016). Typically, analytical precision was better than 4% and detection limits (DL) were 2 µM and 10 µM for CH_4 and CO_2, respectively. The $^{13}C/^{12}C$ abundance ratios of CH_4 and CO_2 (volume of gas injected: 70–500 µL from the headspace) were determined with an Agilent 6890N gas chromatograph (Rt-QPLOT column at 30°C with 99.998% purity He as carrier gas; 3.0 mL min^{-1}) coupled to an Isoprime GVI Isotope Ratio Mass Spectrometer via a combustion interface (Cu(II) oxides, Ni oxides, and a Pt wire). The results are reported as:

$$\delta^{13}C = 1000\left(\frac{\left(\frac{^{13}C}{^{12}C}\right)_{sample}}{\left(\frac{^{13}C}{^{12}C}\right)_{standard}} - 1\right) \quad (1)$$

where ^{13}C and ^{12}C are the abundances of the isotopically heavy and light solute (CH_4 or DIC), respectively, and the reference standard is Vienna Pee Dee Belemnite (VPDB). Two reference gases were used for calibration: CO_2 ($\delta^{13}C = -32.86 \pm 0.10$‰ VPDB; 99.998% purity, Praxair) and CH_4 ($\delta^{13}C = -40.90 \pm 0.17$‰ VPDB; 99.5% purity, Praxair). Both reference gases were previously calibrated at the Laboratory for Light Stable Isotope Geochemistry at UQÀM (courtesy of Dr. J.-F. Hélie) against international standards: LSVEC and NBS-18 for CO_2, and LSVEC and NBS-19 for CH_4. The precision of repeated analysis was typically ± 0.2‰ when 25 µmol of an equimolar gas mixture of CH_4 and CO_2 was injected. The results are generally given as the $\delta^{13}C$ of CH_4 ($\delta^{13}C$-CH_4) and DIC ($\delta^{13}C$-DIC) and, when required, the $\delta^{13}C$ of gaseous CO_2 ($\delta^{13}CO_2$) was calculated from the $\delta^{13}C$-DIC according to Hélie (2004) and Mook et al. (1974).

The CH_3D/CH_4 ratio was determined in only two samples per peeper, collected below 7 cm, with an Agilent 6890 gas chromatograph (Agilent J&W GS-CarbonPLOT column at room temperature) coupled to a Thermo Finnigan Delta+ XL Isotope Ratio Mass Spectrometer via a pyrolysis reactor (ceramic tube at 1450°C). The results were reported according to the δ^2H notation (as for $\delta^{13}C$ in Eq. 1) against the Standard Mean Ocean Water (SMOW) and were corrected with regard to the mean δ^2H of water (−75‰; Timsic and Patterson, 2014) according to Chanton et al. (2006). Isotopically distinct methane standards (Isometric Instruments, Victoria, BC, Canada) were used for calibration. The precision of replicate injections was better than 2.5‰. Acetate

concentrations were obtained by ion chromatography (Dionex IONPAC AS14 Suppressed Conductivity ASRS-II) with a detection limit of 0.5 µM. Concentrations of the other solutes were determined as described by Laforte et al. (2005).

2.3. Thermodynamic and inverse modeling of porewater solutes

The speciation of porewater solutes was calculated with the equilibrium computer program Windermere Humic Aqueous Model (WHAM 6; Tipping, 2002), assuming that all dissolved OM is humic substances, as described in Clayer et al. (2016). Saturation index values (SI = log IAP/K_s, where IAP is the ion activity product and K_s is the solubility product), were calculated with the output IAP values from WHAM 6 and the K_s values from Stumm and Morgan (1996).

The porewater profiles of CH_4 and DIC were modeled with the one-dimensional diagenetic reaction-transport equation for solutes (Boudreau, 1997), assuming steady state and negligible solute transport by bioturbation, bioirrigation and advection in the studied sporadically anoxic basin (Clayer et al., 2016):

$$\frac{\partial}{\partial x}\left(\varphi D_s \frac{\partial [\text{solute}]}{\partial x}\right) + R_{net}^{solute} = 0 \qquad (2)$$

In Eq. (2), [solute] denotes a solute concentration, x is depth (positive downward from the SWI), φ is porosity, D_s is the solute effective diffusion coefficient in sediments, and R_{net}^{solute} (in mol cm^{-3} of wet sediments s^{-1}) is the solute net production rate (or consumption rate if R_{net}^{solute} is negative). Equation (2) was solved for $R_{net}^{CH_4}$ and R_{net}^{DIC} with the computer code PROFILE (Berg et al., 1998), using as input values the measured φ, average (n = 3) CH_4 and DIC profiles and D_s, which was assumed to be $\varphi^2 D_w$, where D_w is the solute tracer diffusion coefficient in water (Ullman and Aller, 1982). The boundary

conditions were the solute concentrations at −0.5 and 22.5 cm. The D_w values were 9.50×10^{-6} cm^2 s^{-1} for CH_4 after correction for in situ temperature (4°C) with an Arrhenius-type equation (Wilke and Chang, 1955; Hayduk and Laudie, 1974; Jähne et al., 1987; Oelkers, 1991), as well as 6.01×10^{-6} cm^2 s^{-1} for HCO_3^- and 1.12×10^{-5} cm^2 s^{-1} for CO_2 after temperature correction with a power law equation (Zeebe, 2011). For DIC, we used a composite D_w value that took into account the relative proportions of HCO_3^- and dissolved CO_2 concentrations. PROFILE yields a vertical discontinuous distribution of constant R_{net}^{solute} values over depth intervals (zones) where a solute is produced or consumed as well as its diffusive flux (J_D) across the SWI. Discrepancies were observed among some of the replicate profiles of CH_4, DIC, SO_4^{2-} and Fe that can be assigned mainly to sediment horizontal heterogeneity (see section 3.1). Since our goal is not to study the effect of sediment patchiness, we choose to model the average rather than the individual profiles of these solutes. Also, attempts to model individual profiles occasionally predicted unrealistic production or consumption zones, a problem associated with a high sensitivity to small variations in concentration data when modeling profiles comprising a low number of data points (Lettmann et al., 2012). Averaging the three profiles smoothened the data and resulted in more coherent R_{net}^{solute} profiles. Additional R_{net}^{solute} values were obtained by modeling the average profiles whose values were increased or decreased by one standard deviation. Comparison of these latter R_{net}^{solute} values with those obtained by modeling the average profiles provides an estimation of the variability in R_{net}^{solute} related to heterogeneity within the 25 m^2 sampling area, which is generally below 5 fmol cm^{-3} s^{-1}.

2.4. Reaction network

The main reactions considered in OM mineralization during early diagenesis of sediment are listed in Table 1. Under oxidant-depleted conditions, fermentation of metabolizable OM of general formula $C_xH_yO_z$ can yield acetate, CO_2 and H_2 (r_1). Note that reaction r_1 takes into account any source of CO_2 during fermentation including the partial degradation of high molecular weight OM (HMW OM) into lower molecular weight OM (LMW OM; Corbett et al., 2013; Corbett et al., 2015). The products of this reaction yield CH_4 via either acetate fermentation (r_2) or hydrogenotrophy (r_3). In addition, when electron acceptors (EAs), i.e., Fe(III), SO_4^{2-}, and partially oxidized HS, are present, CH_4 (r_4) and OM (r_5) can be oxidized to produce CO_2. Here, nitrate and Mn oxyhydroxides were not considered as oxidants owing to the very low concentration of the former (< 2 µmol L^{-1}) over the whole sampling interval and because Mn oxyhydroxides do not form under the slightly acidic conditions prevailing in these porewaters (Chappaz et al., 2008). In addition, we neglected precipitation and dissolution of carbonate minerals except for siderite precipitation (r_6) due to its positive SI values ($SI \geq 0.5$).

According to the reactions listed in Table 1, the $R_{net}^{CH_4}$ in the sediments is given by:

$$R_{net}^{CH_4} = R_2 + R_3 - R_4 \quad (3)$$

where R_2 and R_3 are the rates of CH_4 production due to acetate fermentation (r_2) and hydrogenotrophy (r_3), respectively; and R_4 is the rate of CO_2 production due to CH_4 oxidation (r_4). For its part, the R_{net}^{DIC} can be expressed as:

$$R_{net}^{DIC} = R_1 + R_2 - R_3 + R_4 + R_5 - R_6 \quad (4)$$

where R_1 and R_5 are the rates of CO_2 production due to OM fermentation (r_1) and oxidation (r_5), respectively, and R_6 is the rate of siderite precipitation (r_6).

3. RESULTS

3.1. Profiles of solute concentrations

The replicate depth distributions of CH_4, $\delta^{13}C$-CH_4, DIC, $\delta^{13}C$-DIC, SO_4^{2-}, ΣS(−II) and Fe are shown in Fig. 1. The profiles do not display sharp discontinuities and the main vertical variations are defined by several data points, which suggests that differences among triplicate profiles should be mainly attributed to spatial variability within the 25 m^2 sampling area and not to sampling and handling artefacts. Small-scale sediment patchiness is common in lakes (e.g., Downing and Rath, 1988; Brandl et al., 1993). Profiles of acetate are not shown because concentrations were < 2 µM over the entire sampling interval. Figure 1 also shows sharp CH_4, DIC and Fe gradients above the SWI, indicating diffusion-dominated transport in stagnant overlying water, a feature not unusual in this lake basin (Clayer et al., 2016).

In the overlying water, SO_4^{2-} concentrations are seven times lower than those measured in the epilimnetic waters (Alfaro-De La Torre, 2001), and some of the ΣS(−II) concentrations are significantly higher than the detection limit (i.e., 0.02 µM, Fig. 1h), as often found when SO_4^{2-} reduction occurs in anoxic waters. Below the SWI, ΣS(−II) concentrations decrease and then remain relatively constant at a low concentration of 0.05 ± 0.02 µM, and SO_4^{2-} concentrations remain lower than 3 µM (filled squares and circles in Fig. 1g), except for one profile (filled triangles in Fig. 1g) where they increase with depth to a maximum at about 15 cm. The Fe profiles show sharp positive (top 3 cm)

and negative (between 2 and 5 cm) concentration gradients (Fig. 1i) which indicate dissolved Fe production and consumption, respectively. Below 5 cm depth, the concentrations progressively increase with depth.

The concentrations of CH_4, which increase with depth from 0.2–0.5 mM in the overlying water to 1.2–1.4 mM at the base of the profiles (Fig. 1a–c), are well below saturation, i.e., 7.1 mM at 4°C and in situ pressure (Duan and Mao, 2006), suggesting that ebullition is a negligible transport process. The CH_4 profiles follow two distinct patterns (Fig. 1a–c). Those represented by circles and squares consistently show a concave-up curvature between 0 and 5–6 cm depth and a concave-down curvature below, whereas that symbolized by triangles displays a concave-down curvature over the entire sediment column. This disparity, also observed for the other solute concentrations and $\delta^{13}C$ data, where the profile represented by triangles is always different from the two others (Fig. 1), can be attributed to the heterogeneity at the study site (Brandl et al., 1993).

The CH_4 concentration profile calculated with the code PROFILE accurately fits the average (n = 3) measured data ($r^2 > 0.998$; Fig. 2a) and predicts a diffusive flux of CH_4 ($J_D^{CH_4} = -0.4$ pmol cm^{-2} s^{-1}) to the bottom water. The $R_{net}^{CH_4}$ profile shows a zone of net CH_4 consumption ($Z_c^{CH_4}$; $R_{net}^{CH_4} = -23$ fmol cm^{-3} s^{-1}) above two zones of net production, one located between 5 and 7.5 cm depth ($Z_{p1}^{CH_4}$; $R_{net}^{CH_4} = 116$ fmol cm^{-3} s^{-1}) and the other below 7.5 cm depth ($Z_{p2}^{CH_4}$; $R_{net}^{CH_4} = 11$ fmol cm^{-3} s^{-1}). The $Z_c^{CH_4}$ and $Z_{p1}^{CH_4}$ can be combined into a single zone of net CH_4 production by forcing the code PROFILE to rationalize the average CH_4 profile with only two zones instead of three, but it significantly reduces the quality of the fit. Indeed, the P value (0.000) obtained by

statistical F-testing at a level of significance ≤ 0.001 shows that the $R_{net}^{CH_4}$ profile with three zones is significantly better than that with only two zones.

The concentrations of DIC, as those of CH_4, increase steadily between the overlying water and 23 cm depth (Fig. 1e). The code PROFILE generates a curve that fits accurately the average (n = 3) experimental DIC data ($r^2 > 0.998$; Fig. 2b) and it predicts that the diffusive flux of DIC (J_D^{DIC}) to the overlying water is -1.1 pmol cm^{-2} s^{-1}. It defines three zones of net DIC production or consumption numbered Z_1^{DIC}, Z_2^{DIC} and Z_3^{DIC} from the sediment surface (Fig. 2b). Two zones of net DIC production (Z_1^{DIC} and Z_2^{DIC} where R_{net}^{DIC} is equal to 138 fmol cm^{-3} s^{-1} and 42 fmol cm^{-3} s^{-1}, respectively) occur above a zone of net DIC consumption (Z_3^{DIC}, with $R_{net}^{DIC} = -13$ fmol cm^{-3} s^{-1}). Note that the boundary between $Z_c^{CH_4}$ and $Z_{p1}^{CH_4}$ does not match exactly that between Z_1^{DIC} and Z_2^{DIC}.

As a check of the robustness of the $R_{net}^{CH_4}$ and R_{net}^{DIC} depth distributions predicted by PROFILE, the average CH_4 and DIC profiles were also modeled using another inverse modeling code, i.e., Rate Estimation from Concentrations (REC, Lettmann et al., 2012). The REC code uses a statistical approach, the Tikhonov regularization technique, which differs from that used by PROFILE. Figure S1 in the Supplementary Material shows that the two codes predicted coherent rate profiles with the same number of zones, except for the two consecutive zones of DIC net production predicted by PROFILE, which are predicted by REC as a single zone of decreasing intensity. Moreover, the values of the net rates are of similar magnitude.

3.2. Profiles of $\delta^{13}C$-CH_4 and $\delta^{13}C$-DIC

The $\delta^{13}C$ values increase with sediment depth from −74.2 ± 1.0‰ to −70.7 ± 0.9‰ for CH_4 (Fig. 1d) and from −13 ± 2.9‰ to +5.1 ± 0.9‰ for DIC (Fig. 1f). The values of $\delta^{13}C$-CH_4, which are smaller than −70‰ over the whole sediment column, as well as the large difference between the $\delta^{13}C$ of CO_2 gas ($\delta^{13}CO_2$) and $\delta^{13}C$-CH_4 (68–82‰), suggest that hydrogenotrophy is the main methanogenic pathway at our sampling site (Whiticar, 1999). These values differ from those reported for acetoclastic methanogenesis ($\delta^{13}C$-CH_4 from −68 to −50‰ and $\delta^{13}CO_2 - \delta^{13}C$-$CH_4$ from 39 to 58‰; Whiticar, 1999). The concomitant increase with depth of $\delta^{13}C$-CH_4 and $\delta^{13}C$-DIC is consistent with a dominance of hydrogenotrophic methanogenesis. It should be noted that except for two data points (filled circles in Fig. 1d), the $\delta^{13}C$-CH_4 signatures do not shift toward higher values in the $Z_c^{CH_4}$ or above the SWI (Figs. 1d and 3), a feature that is discussed in section 4.1.3. As shown in Fig. 3, the signature of all our samples falls within the CO_2 reduction domain in a $\delta^{13}CO_2$– $\delta^{13}C$-CH_4 graph. Also, the $\delta^{2}H$ of CH_4 (−160 to −183‰ SMOW) is typical of CH_4 produced by CO_2 reduction (Whiticar, 1999).

4. DISCUSSION

4.1. Pathways of OM degradation

Plotting the experimental data on the $\delta^{13}CO_2$ *vs.* $\delta^{13}C$-CH_4 graph proposed by Whiticar (1999; see Fig. 3) allows performing a quick diagnosis of the main methanogenic and methanotrophic pathways but is insufficient to quantify the relative contribution of each reaction involved in OM mineralization. To reach this goal, we select from Table 1 the reactions that are plausible in each zone, constrain their rates

using the $R_{net}^{CH_4}$ and R_{net}^{DIC} values reported in Table 2, and assign a rate value of 0 to the reactions that are unlikely to occur. The sets of reaction rates thus established for r_1 to r_6 in each zone, when combined for the $Z_c^{CH_4}$, $Z_{p1}^{CH_4}$ and $Z_{p2}^{CH_4}$, provide scenarios to predict the δ^{13}C-CH_4 and δ^{13}C-DIC profiles with a one-dimensional diagenetic reaction-transport equation. The comparison between the measured and simulated δ^{13}C-CH_4 and δ^{13}C-DIC profiles allows to propose the most probable scenario and to quantify the contribution of each reaction to OM degradation. The diagenetic equation, conversely to the Rayleigh model, takes into account the influence of transport processes on the depth distribution of isotope ratios, and it is better suited from a theoretical point of view for constraining fractionation factors and diffusivity coefficients in sediments (Alperin et al., 1988).

4.1.1. Constraining the rates of OM mineralization reactions

In the $Z_c^{CH_4}$ (i.e., between the SWI and 5 cm depth), DIC is produced through both OM oxidation and methanotrophy as revealed by the R_{net}^{DIC} value greater than that of $-R_{net}^{CH_4}$ (Table 2). For now, we assume that fermentation and methanogenesis are negligible in the $Z_c^{CH_4}$, i.e., $R_1 = R_2 = R_3 = 0$, since these processes should only occur when EAs are absent (Bridgham et al., 2013). Shortage of EAs is unlikely because the porewater Fe profiles (Fig. 1i) reveal some Fe oxyhydroxide reduction in the $Z_c^{CH_4}$, between 0 and 2 cm. In addition, below that depth interval, within the same zone, the Fe profiles display evidence of porewater Fe consumption, and SI values in that zone (SI ≥ 0.5) indicate that porewater is supersaturated with respect to siderite. Modeling the average Fe concentration profiles with the code PROFILE yields a net Fe consumption rate of −34 fmol cm^{-3} s^{-1} over the $Z_c^{CH_4}$ which is considered below as an estimate of the

rate of siderite precipitation, i.e., $R_6 = -34$ fmol cm^{-3} s^{-1}. With thie assumption stated above, the only reactions thus occurring in that zone are r_4, r_5 and r_6. Consequently, Eq. 3 simplifies to $R_4 = -R_{net}^{CH_4} = 23$ fmol cm^{-3} s^{-1} and, from Eq. 4, we obtain that $R_5 = R_{net}^{DIC} + R_{net}^{CH_4} - R_6 = 125$ fmol cm^{-3} s^{-1} (Table 2). The effect of adding methanogenesis to OM oxidation, methanotrophy and siderite precipitation in the $Z_c^{CH_4}$ is discussed below in section 4.1.3.

In the $Z_{p1}^{CH_4}$ (i.e., between 5 and 7.5 cm depth), which is the zone with the most elevated net CH_4 production rate, CH_4 and DIC are simultaneously produced but the value of $R_{net}^{CH_4}$ is more than twice that of R_{net}^{DIC} (Fig. 2 and Table 2). Note that this observation is consistent with our previous study at the same site showing similar values for the CH_4 to DIC net rate ratios ($R_{net}^{CH_4}/R_{net}^{DIC}$ of 2 to 4) in the sediment methanogenic zone (Clayer et al., 2016). We assume that reactions r_4, r_5 and r_6 are not significant sources or sink of DIC, i.e., $R_4 = R_5 = R_6 = 0$, leaving only reaction r_1–r_3 as plausible reactions in the $Z_{p1}^{CH_4}$. This assumption is based on the facts that nitrate and Mn oxyhydroxides can be neglected as oxidants (see section 2.4) and that the porewater profiles of SO_4^{2-} and Fe display only slight concentration variations within the 5–7.5 cm depth interval (Fig. 1g and i). Modeling these profiles with Eq. 2 (data not shown) indicates that there is no net SO_4^{2-} consumption ($R_{net}^{SO_4^{2-}} > 0$) in the $Z_{p1}^{CH_4}$ and that the net rate of dissolved Fe production in that zone (i.e., $R_{net}^{Fe} = 0.1$ fmol cm^{-3} s^{-1}), from which we may infer some Fe(III) reduction, is more than two orders of magnitude lower than that of the net rate of DIC production.

To avoid the complexity of testing a large number of hydrogenotrophy and acetate fermentation proportions for the CH_4 production in the $Z_{p1}^{CH_4}$, we consider two extreme cases (or end-members). For one of them, we postulate that methanogenesis proceeds exclusively through hydrogenotrophy, i.e., $R_2 = 0$. In that case, r_1 produces only CO_2 and H_2, but no acetate (i.e., x = ν in reaction r_1), and we obtain, from Eq. 3, that $R_{net}^{CH_4} = R_3 = 116$ fmol cm^{-3} s^{-1} and, by adding Eqs. 3 and 4, that $R_1 = R_{net}^{DIC} + R_{net}^{CH_4} = 158$ fmol cm^{-3} s^{-1}. In the other extreme case, we constrain the maximum proportion of CH_4 produced by acetate fermentation with the measured values of $R_{net}^{CH_4}$ and R_{net}^{DIC} considering that all DIC is produced by this process, i.e., r_1 produces only acetate and H_2 (ν = 0 in reaction r_1 and $R_1 = 0$). By adding Eqs. 3 and 4, we obtain $R_2 = \frac{R_{net}^{DIC} + R_{net}^{CH_4}}{2} = 79$ fmol cm^{-3} s^{-1} and, from Eq. 3, that $R_3 = 37$ fmol cm^{-3} s^{-1}. In this extreme case (or end-member), the proportions of the total CH_4 production through acetate fermentation and hydrogenotrophy are 68% (i.e., $\frac{R_2}{R_2+R_3}$) and 32% (i.e., $\frac{R_3}{R_2+R_3}$), respectively.

Lastly, in the $Z_{p2}^{CH_4}$ (i.e., 7.5–22.5 cm depth), the net production rate of CH_4 and the net consumption rate of DIC have a similar value (i.e., 11–13 fmol cm^{-3} s^{-1}; Table 2) suggesting that hydrogenotrophy (r_3) is the only reaction taking place in that zone. The presence of DIC in the $Z_{p2}^{CH_4}$ is likely due to its diffusion from deeper porewater and perhaps from the $Z_{p1}^{CH_4}$ (Fig. 2c), but not to its production through the reactions listed in Table 1. Since there is no evidence of siderite precipitation in that zone (i.e., $R_6 = 0$), and assuming that $R_1 = R_2 = R_4 = R_5 = 0$, it can be written from Eqs. 3 and 4 that

$R_3 = 12$ fmol cm^{-3} s^{-1}. Note that the origin of the substrate H_2 required for hydrogenotrophy is discussed below.

The values of the reaction rates R_1–R_6 evaluated as described above in the three zones defined by our modeling, are combined in order to provide two scenarios (S1 and S2) of reaction rates for the top 25 cm of Lake Tantaré sediments (see Table 2). While only one set of reaction rates is realistic for each of the $Z_c^{CH_4}$ and the $Z_{p2}^{CH_4}$, two sets are considered for the $Z_{p1}^{CH_4}$, corresponding to the maximum (S1) and minimum (S2) proportion of hydrogenotrophy. Below, the $\delta^{13}C$ profiles of CH_4 and DIC are simulated according to these scenarios.

4.1.2. Modeling the δ^{13}C-CH_4 and δ^{13}C-DIC profiles

To model the $\delta^{13}C$ profiles of CH_4 and DIC, we use Eq. 1 modified as follows:

$$\delta^{13}\mathrm{C} = 1000\left(\frac{\left(\frac{[^{13}\mathrm{C}]}{[\mathrm{C}]}\right)_{\mathrm{sample}}}{\left(\frac{^{13}\mathrm{C}}{^{12}\mathrm{C}}\right)_{\mathrm{standard}}} - 1\right) \qquad (5)$$

where $[\mathrm{C}]$ is the total CH_4 or DIC concentration, which is an approximation of the isotopically light concentrations of these solutes, given that ~99% of total carbon is made of ^{12}C (Faure, 1998), and $[^{13}\mathrm{C}]$ is the isotopically heavy CH_4 or DIC concentration. Equation 5 allows calculating $\delta^{13}C$ once $[^{13}\mathrm{C}]$ and $[\mathrm{C}]$ are known. A numerical representation of the $[\mathrm{C}]$ depth distribution is given by Eq. 2, whereas that for $[^{13}\mathrm{C}]$ is obtained by an adapted version of Eq. 2 (Alperin et al., 1988), in which $[\mathrm{solute}]$ is

replaced by $[^{13}C]$ and R_{net}^{solute} by the net reaction rate of the isotopically heavy solute ($R_{net}^{*solute}$):

$$\frac{\partial}{\partial x}\left(\varphi \frac{D_s}{f}\frac{\partial[^{13}C]}{\partial x}\right) + R_{net}^{*solute} = 0 \qquad (6)$$

where f, the molecular diffusivity ratio, is the diffusion coefficient of the total solute divided by that of the isotopically heavy solute (Table 3). In Eq. 6, $R_{net}^{*solute}$ is the sum of the reaction rates of the isotopically heavy solute in reactions r_1–r_6 (Table 1), i.e.,

$$\sum_{i=1}^{6} R_i^*$$

. The rate R_i^* can be expressed as follows (Rees, 1973):

$$R_i^* = \frac{R_i[^{13}C]_i^{reactant}}{\alpha_i[C]_i^{reactant}} \qquad (7)$$

where α_i is the isotopic fractionation factor, $[C]_i^{reactant}$ and $[^{13}C]_i^{reactant}$ are the total concentrations of a reactant and that of its isotopically heavy component, respectively, and R_i is the solute reaction rate in reaction r_i. Substituting Eq. 7 into Eq. 6, we obtain:

$$\frac{\partial}{\partial x}\left(\varphi \frac{D_s}{f}\frac{\partial[^{13}C]}{\partial x}\right) + \sum_{i=1}^{6}\frac{R_i[^{13}C]_i^{reactant}}{\alpha_i[C]_i^{reactant}} = 0 \qquad (8)$$

Introducing the definition of $\delta^{13}C_i^{reactant}$, i.e., the $\delta^{13}C$ of the reactant in reaction r_i leading to the formation of the solute (CH_4 or DIC), into Eq. 8 leads to:

$$\frac{\partial}{\partial x}\left(\varphi \frac{D_s}{f}\frac{\partial[^{13}C]}{\partial x}\right) + \sum_{i=1}^{6}\frac{R_i}{\alpha_i}\left(\frac{\delta^{13}C_i^{reactant}}{1000}+1\right)\left(\frac{^{13}C}{^{12}C}\right)_{standard} = 0 \qquad (9).$$

Equation 2 was solved numerically for [C] via the `bvp5c` function of MATLAB® using D_s, the measured φ, and $R_{net}^{CH_4}$ or R_{net}^{DIC} in the $Z_c^{CH_4}$, $Z_{p1}^{CH_4}$ and $Z_{p2}^{CH_4}$ as inputs, and, CH_4 or DIC concentrations at the top and bottom of the profiles as boundary conditions. It should be noted that the value of R_{net}^{DIC} in the $Z_c^{CH_4}$ used for the calculations was a weighted average of the two R_{net}^{DIC} values provided by PROFILE in that zone (Fig. 2b, Table 2). The CH_4 and DIC profiles simulated this way were very similar to those generated by the code PROFILE (Fig. 2a and b), thus validating our script.

With regard to Eq. 9, it was solved for $[^{13}C]$ via the `bvp5c` function of MATLAB®, using D_s, φ, R_i, $\delta^{13}C_i^{reactant}$, α_i and f as inputs, and the $[^{13}C]$ values at the top and bottom of the profiles calculated with Eq. 5 as boundary conditions. The values of R_i were those reported in Table 2 for scenarios S1 and S2. The values of $\delta^{13}C_i^{reactant}$ were −28‰ for OM (Joshani, 2015), −38‰ and −18‰ for the methyl and carboxyl groups of acetate (Conrad et al., 2014), respectively, and the measured values of δ^{13}C-CH_4 and δ^{13}C-DIC. We assumed no isotope fractionation during CO_2 production through OM fermentation and oxidation (i.e., $\alpha_1 = \alpha_5 = 1.000$) as reported in many studies (Lapham et al., 1999; Fey et al., 2004; Werth and Kuzyakov, 2010; Conrad et al., 2012). Considering the large ranges of values reported in the literature for α_2, α_3 and α_4, estimated values, hereafter referred to as default values, were selected for initial simulations. Methane produced by acetate fermentation (r_2) is typically depleted in ^{13}C by 21–27‰ (i.e., α_2-CH_4 varies between 1.021 and 1.027) compared to its substrate, the methyl group of acetate (Krzycki et al., 1987; Gelwicks et al., 1994; Whiticar, 1999; Conrad, 2005), and CO_2 production through acetoclastic methanogenesis appears to undergo similar ^{13}C depletion (Blair and Carter, 1992; Gelwicks et al., 1994).

Consequently, the same intermediate fractionation factor was chosen as default values for α_2-CH_4 and α_2-CO_2 i.e., 1.024. Hydrogenotrophy is known to generate a larger fractionation than acetate fermentation with α_3 values ranging from 1.050 to 1.095 (Whiticar, 1999; Conrad, 2005). In agreement with Conrad et al. (2014), we used 1.075 as the default value for α_3. As regard α_4, a default value of 1.005 was selected as in Whiticar and Faber (1986) and in agreement with other studies showing that α_4 may vary from 1.005 to 1.031 (Alperin et al., 1988; Whiticar, 1999). For siderite precipitation, we calculated a composite α_6 value using the fractionation factors reported for calcite precipitation from aqueous CO_2 (0.990) or HCO_3^- (0.998) solutions and taking into account the relative proportions of porewater HCO_3^- and CO_2 concentrations (Bottinga, 1969; Emrich et al., 1970).

Isotopic fractionation due to diffusion depends on the mass and on the interaction among solute molecules and water (Jähne et al., 1987). The strong interactions between DIC and water lowers the theoretical kinetic fractionation effect resulting in an f-DIC value lower than 1.001 (O'Leary, 1984; Jähne et al., 1987). In contrast, a relatively higher value is expected for f-CH_4 because of the relatively large mass difference between $^{13}CH_4$ and $^{12}CH_4$ compared with that between $^{13}CO_2$ and $^{12}CO_2$, and the weaker interactions between CH_4 and water due to the hydrophobic character of CH_4. The value of f–CH_4 was estimated to be less than 1.003 at the water-air interface (Happell et al., 1995), which can be considered as a maximum value in sediments. We thus chose 1.000 as default value for f-CH_4 and f-DIC. After performing the initial simulation, the values of f-CH_4, as well as those of α_2, α_3 and α_4, were then varied within the ranges reported in the literature (Table 3) to perform additional simulations.

The depth distributions of $[C]$ and $[^{13}C]$ were combined in Eq. 5 to model the $\delta^{13}C$ profiles of CH_4 and DIC, which were visually and statistically compared to the measured profiles to determine what scenario and parameter values best reflect the measurements. The norm of residuals (N_{res}) was used to compare the goodness of fits:

$$N_{res} = \sqrt{\sum_{x=0.5}^{22.5} (\delta^{13}C_m - \delta^{13}C_s)^2} \qquad (10)$$

where $\delta^{13}C_m$ and $\delta^{13}C_s$ are the measured and simulated $\delta^{13}C$ values, respectively. The norm of residuals (N_{res}) varies between 0 and infinity with smaller numbers indicating better fits.

4.1.3. Selecting the best scenario

Figure 4 shows that the $\delta^{13}C$-CH_4 and $\delta^{13}C$-DIC profiles modeled with default parameters result in a better fit of the measured profiles for S1 than for S2. Indeed, the N_{res} values of $\delta^{13}C$-CH_4 (1.09) and $\delta^{13}C$-DIC (1.65) for S1 are lower than those for S2 ($\geq$ 3.70). The search for the best scenario can be taken a step further by investigating the influence of the fractionation factors α_2, α_3, and α_4, and of the molecular diffusivity factor f-CH_4 on N_{res}.

The fit between the measured and modeled $\delta^{13}C$-CH_4 profiles for scenario S2 can be improved by varying α_3 within the range of values given in Table 3, while maintaining the default values for the other parameters; the best fit is obtained with α_3 = 1.087 (N_{res} = 0.84). However, the N_{res} for $\delta^{13}C$-DIC remained above 4.90 regardless of the α_3 value. Varying the other parameters between their maximum and minimum values

reported in Table 3 together with that of α_3 did not significantly improve the δ^{13}C-DIC fit ($N_{res} > 4.00$). We thus conclude that scenario S2 is unrealistic and it is not discussed further.

Figure 5a shows that varying α_3, the most influential fractionation factor for scenario S1, and maintaining the default values for the other parameters, can significantly improve the fit between measured and simulated profiles. However, the minimum value of N_{res} occurs at different α_3 values for the δ^{13}C-CH_4 (α_3 = 1.0764) and the δ^{13}C-DIC (α_3 = 1.0830) profiles, likely due errors associated with the analyses and estimation of the rates. Given that α_3 ought to have the same value for both δ^{13}C-CH_4 and δ^{13}C-DIC, the best fit is considered to occur at the minimum of total N_{res} (the sum of N_{res} for the δ^{13}C-CH_4 and the δ^{13}C-DIC profiles), i.e., at α_3 = 1.0770 in Fig. 5a where total N_{res} is 2.23. Increasing the value of f-CH_4 from 1.000 to 1.003 and that of α_4 from 1.005 to 1.016 further lowers the minimum total N_{res} value to 1.89 at α_3 = 1.081. This latter value of total N_{res} correspond to the best fit of the modeled profiles that we can obtain for S1.

The better fit for S1 compared to S2 agrees with the predominance of hydrogenotrophy in CH_4 production in Lake Tantaré sediments, but to estimate more precisely the contribution of acetate fermentation to methanogenesis, additional simulations were performed by varying the proportion of acetoclastic methanogenesis in the $Z_{p1}^{CH_4}$ from 0 (as in S1) to 25%. For each proportion of acetoclastic methanogenesis tested, the values of α_2, α_3, α_4 and f-CH_4 were optimized, as done for S1. Increasing the proportion of acetate fermentation slightly lowers the N_{res} values of the δ^{13}C-CH_4 fit but

increases considerably that of the δ^{13}C-DIC fit (Fig. 5b), which indicates that the contribution of acetate fermentation is negligible in the $Z_{p1}^{CH_4}$.

The value of α_3 yielding the best fit (1.081) is well within the range reported in the literature (Table 3). This value is slightly higher than that (1.075) estimated from incubation experiments usually performed at temperatures above 20°C (Conrad et al., 2014). The lower temperature (4°C) at the study site could explain our slightly greater α_3 value since this fractionation factor is reported to decrease with temperature (Richet et al., 1977; Whiticar et al., 1986). Lastly, our optimal value for α_4 (1.016) is within the range reported for aerobic CH_4 oxidation (Barker and Fritz, 1981). However, it remains poorly constrained considering that only a minor fraction of CH_4 is consumed through oxidation in the $Z_c^{CH_4}$.

Methanogenesis in the $Z_c^{CH_4}$ needs to be invoked to explain the upward decrease in δ^{13}C-CH_4 in that zone, which is at odds with the assumption that $R_1 = R_2 = R_3 = 0$ made in developing S1 and S2 (section 4.1.1.). Strong ^{13}C-CH_4 depletion is often observed near the base of the sulfate methane transition zone, where CH_4 is consumed via SO_4^{2-} reduction in marine sediments (Borowski et al., 1997; Martens et al., 1999; Pohlman et al., 2008; Treude et al., 2014). This feature, which is counterintuitive since the CH_4 left behind during methanotrophy should be ^{13}C-enriched, has been attributed to the production of CH_4 by hydrogenotrophy from the ^{13}C-depleted DIC resulting from anaerobic CH_4 oxidation (Borowski et al., 1997; Pohlman et al., 2008). In our case, we suggest that the ^{13}C-CH_4 depletion in the $Z_c^{CH_4}$ results mainly from reduction of ^{13}C-depleted DIC originating from the oxidation of OM ($\delta^{13}C = -28‰$; Joshani 2015), the

main source of DIC in that zone (Table 2). This contention is supported by: i) the positive correlation between δ^{13}C-CH_4 and δ^{13}C-DIC in the $Z_c^{CH_4}$ (Fig. 2 c and d), ii) the δ^{13}C values for CH_4 (−74 to −72‰) and CO_2 gas (−2 to 6‰) in that zone which plot in the hydrogenotrophy domain in Fig. 3, and iii) the difference between $\delta^{13}CO_2$ and δ^{13}C-CH_4 (68–73‰) which is typical of hydrogenotrophy (Whiticar, 1999). Note that this difference is smaller in the $Z_c^{CH_4}$ than in the $Z_{p1}^{CH_4}$ and $Z_{p2}^{CH_4}$ (74–83‰) in which hydrogenotrophy is the main reaction, suggesting that methanotrophy is occurring in addition to hydrogenotrophy in the $Z_c^{CH_4}$. Sediments are naturally heterogeneous and microenvironments of redox potential lower than that of the bulk sediment, where OM fermentation and hydrogenotrophy could occur, are likely present in the $Z_c^{CH_4}$. A small contribution of hydrogenotrophy would probably be sufficient to counterbalance the ^{13}C-CH_4 enrichment expected from methanotrophy and produce the observed net ^{13}C-CH_4 depletion since isotopic fractionation is much greater for hydrogenotrophy than for methanotrophy. Adding hydrogenotrophy in the $Z_c^{CH_4}$ at rates of up to 30 fmol cm^{-3} s^{-1}, i.e., up to 55% of the rate of methanotrophy, slightly worsens the fits of the measured δ^{13}C-CH_4 and δ^{13}C-DIC ($N_{res} \leq 1.94$) compared to those obtained for S1 (N_{res} =1.89). Also, only minor changes in the values of the fractionation factors were required to optimize the fits when adding hydrogenotrophy. The optimized α values remain within the ranges given in Table 3. In addition, the total N_{res} increased when acetoclastic methanogenesis was added, as it was the case when hydrogenotrophy was neglected in the $Z_c^{CH_4}$.

4.2. Sources of H_2 in the zones of CH_4 production

The dominant substrates in fermentation, often inferred to be polysaccharides (Conrad, 1999), are commonly represented in geochemical models by the simple molecule CH_2O (Van Cappellen and Wang, 1996; Canavan et al., 2006; Conrad et al., 2009; Conrad et al., 2010; Galand et al., 2010; Corbett et al., 2013; Aller, 2014; Arning et al., 2016), whose complete fermentation, coupled to methanogenesis, yield equimolar amounts of CH_4 and CO_2. The fermentation of CH_2O, coupled to hydrogenotrophy, cannot alone explain the facts that $R_{net}^{CH_4}$ is about three times greater than R_{net}^{DIC} in the $Z_{p1}^{CH_4}$, and that DIC is consumed at about the same rate as CH_4 is produced in the $Z_{p2}^{CH_4}$ (Table 2). Additional H_2 production is thus required at rates of 148 fmol cm^{-3} s^{-1} and of 48 fmol cm^{-3} s^{-1}, i.e., four times the missing CH_4 production rate of $1/2\left(R_{net}^{CH_4} - R_{net}^{DIC}\right)$, in the $Z_{p1}^{CH_4}$ and $Z_{p2}^{CH_4}$, respectively. The importance of a cryptic Fe-S cycle (Mills et al., 2016) and of the fermentation of organic substrates which are more reduced than CH_2O, as possible pathways of additional H_2 production, are discussed below.

4.2.1. The importance of a cryptic Fe-S cycle

The reduction of Fe oxyhydroxides coupled to the oxidation of reduced sulfur, also referred to as a cryptic Fe-S cycle (Bottrell et al., 2000; Holmkvist et al., 2011a; Holmkvist et al., 2011b; Mills et al., 2016), could produce some H_2:

$$17H_2S + 8FeOOH \xrightarrow{R_7} SO_4^{2-} + 8FeS_2 + 8H_2 + 12H_2O + 2H^+ \quad (11)$$

$$16H_2S + 8FeOOH \xrightarrow{R_8} 8FeS_2 + 4H_2 + 16H_2O \quad (12)$$

where R_7 and R_8 are the rates of solid Fe(III) reduction via reactions 11 and 12, respectively.

Reactions 11 and 12 may occur in the sediment below the $Z_c^{CH_4}$ as revealed by the progressive downward increases in dissolved Fe (Fig. 1i) and of SO_4^{2-} (Fig. 1g) with depth, which suggests that solid-phase Fe(III) reduction continues to be effective below the $Z_c^{CH_4}$, and that SO_4^{2-} is coincidently produced as in reaction 11. However, as estimated in other studies (Liu et al., 2015; Clayer et al., 2016), the rate of solid Fe(III) consumption at our study site is too small, i.e., < 1 fmol cm^{-3} s^{-1}, to provide enough H_2 to sustain the required additional hydrogenotrophy in both the $Z_{p1}^{CH_4}$ and $Z_{p2}^{CH_4}$. Indeed, to match the needed rate of H_2 production, R_7 should be 148 fmol cm^{-3} s^{-1} in the $Z_{p1}^{CH_4}$, and 48 fmol cm^{-3} s^{-1} in the $Z_{p2}^{CH_4}$, whereas R_8 should be twice these values. It may therefore be concluded that, if a cryptic Fe-S cycle is active in Lake Tantaré sediments, it cannot sustain the observed CH_4 production rate.

4.2.2. The importance of reduced OM

Metabolizable organic substrates other than carbohydrates, such as lipids, whose average carbon oxidation states (COS) is lower than 0, are likely abundant enough in sediments (Hedges and Oades, 1997; Burdige, 2006) to contribute significantly to the amount of CH_4 and DIC produced during fermentation. The closer the COS of the fermenting molecules is to that of CH_4 (COS = −4), the larger is the CH_4 : CO_2 production ratio (Arning et al., 2016; Table 4). For example, the complete fermentation of the C_{16}-fatty acid (COS = −1.75) or any fatty alcohol (COS = −2.00) coupled to methanogenesis would yield 2.6–3.0 times more CH_4 than CO_2 (Table 4).

The stoichiometry and the COS of the fermenting OM ($C_xH_yO_z$) can be constrained as follows in the $Z_{p1}^{CH_4}$ where fermentation (r_1) and hydrogenotrophy (r_3) are

coupled. Note that this exercise does not apply to the $Z_{p2}^{CH_4}$ since the substrate DIC required for hydrogenotrophy is not produced in that zone but diffuses from deeper sediments. Considering that methanogenesis is essentially hydrogenotrophic (i.e., x = ν), the reaction of fermentation (r_1) becomes:

$$C_xH_yO_z + (2x - z)H_2O \xrightarrow{R_1} xCO_2 + (2x + \frac{y}{2} - z)H_2 \quad (13)$$

If there is no other source of CO_2, H_2 and CH_4 than the complete fermentation of $C_xH_yO_z$ and hydrogenotrophy, and if we assume that $R_4 = R_5 = R_6 = 0$ (Table 2), the rate of CO_2 production in Eq. 13, i.e., R_1, should be:

$$R_1 = R_{net}^{CH_4} + R_{net}^{DIC} = 158 \text{ fmol cm}^{-3}\text{s}^{-1} \quad (14)$$

and the rate of H_2 production in Eq. 13 required to sustain the rate of CH_4 production by reaction r_3 can be written:

$$\left(\frac{4x + y - 2z}{2x}\right) R_1 = 4R_3 = 4R_{net}^{CH_4} \quad (15)$$

Introducing into Eq. 15, the values of $R_{net}^{CH_4}$ (116 fmol cm^{-3} s^{-1}; Table 2) and that of R_1 (158 fmol cm^{-3} s^{-1}; Eq. 14), we obtain:

$$y - 2z = 1.87x \quad (16)$$

The COS of an organic molecule is given by:

$$COS = -\sum_i OS_i \frac{n_i}{n_c} \quad (17)$$

where OS_i is the oxidation state of the element *i* and n_i/n_c is its molar ratio to carbon. Assuming that the COS of the fermenting molecule in the $Z_{p1}^{CH_4}$ is defined only by H and O atoms, it can be written:

$$\mathrm{COS} = -\left(\frac{(1.87x + 2z) \times (+1) + (z) \times (-2)}{x}\right) = -1.87 \quad (18)$$

This COS value is closer to those of fatty acids (COS of −1.50 for C_8-fatty acids to about −1.87 for C_{32}-fatty acids) and of fatty alcohols (COS = −2.00) than to that of the commonly assumed model organic molecule CH_2O (COS = 0). Fatty acids are widespread lipid compounds in lake sediments (Cranwell, 1981; Matsumoto, 1989), and the short-chain (up to 20 C) acids are known to be more labile than their long-chain counterparts (Farrington et al., 1977; Matsuda and Koyama, 1977; Matsuda, 1978) with molecules containing 16 C atoms being the most abundant (Cranwell, 1981; Matsumoto, 1989).

From Eq. 16, the general formula for the fermenting OM can be written: $C_xH_{1.87x+2z}O_z$. Given that a carbon chain of x atoms can be bound to a maximum of (2x + 2) H or O atoms, we can write:

$$y + z \leq 2x + 2 \quad (19)$$

Combining Eqs. 16 and 19 leads to:

$$z \leq \frac{0.13x + 2}{3} \quad (20)$$

If we assume that the number of C atoms in the fermenting OM is 16, its formula becomes $C_{16}H_{29.9+2z}O_z$ with $z \leq 1.36$, and the sum of the reactions of fermentation (Eq. 13) and hydrogenotrophy (r_3) could thus be written as follows:

$$C_{16}H_{29.9+2z}O_z + (32 - z)H_2O \rightarrow 16CO_2 + 47H_2 \quad (21)$$

$$11.75CO_2 + 47H_2 \rightarrow 11.75CH_4 + 23.5H_2O \quad r_3$$

$$C_{16}H_{29.9+2z}O_z + (8.5 - z)H_2O \rightarrow 4.25CO_2 + 11.75CH_4 \quad (22)$$

where z can take any value between 0 and 1.36 (Eq. 20).

Equations 18 and 22 were developed with the assumption that there was no other source of CH_4, H_2 and CO_2 than fermentation and hydrogenotrophy in the $Z_{p1}^{CH_4}$. Increasing the rate of methanotrophy, and that of hydrogenotrophy by the same value in order to remain consistent with the measured value of $R_{net}^{CH_4}$ and with Eq. 3, would increase the rate of H_2 production required in Eq. 21 to sustain the CH_4 production rate. More H atoms would thus be required in the chemical formula of the fermenting OM, which would decrease its COS. Considering that EAs are depleted in the $Z_{p1}^{CH_4}$ as discussed in section 4.1.1., and that adding some methanotrophy in that zone would not improve the fit between simulated and measured $\delta^{13}C$ profiles (data not shown), there is no reason to believe that methanotrophy is a significant source of DIC in the $Z_{p1}^{CH_4}$. Lastly, in deriving the COS, we assumed that the fermenting molecules contain only C, H and O. Including other elements (e.g., N and S) would have only a minor effect on the COS value because these elements are not abundant.

Although, the accuracy of the COS value (−1.9) estimated with Eq. 18 is difficult to evaluate, such low COS values can only be explained by the fermentation of fatty acids and alcohols, terpenes or complex reduced organics such as type I kerogen (Kroll et al., 2011; LaRowe and Van Cappellen, 2011). Complex organic molecules are generally considered non-degradable, especially under anoxic conditions (Burdige, 2007). Although it is generally accepted that lipids are less degradable than proteins or carbohydrates (Baldock et al., 2004; LaRowe and Van Cappellen, 2011), several studies showed that fatty acids and sterols are degraded in natural sediments under anoxic conditions (Farrington et al., 1977; Kawamura et al., 1980; Cranwell, 1981; Canuel and Martens, 1996; Harvey and Macko, 1997). We thus submit that once organic particles

reach the sediment floor at our study site, the most easily degradable organic compounds (i.e., proteins and carbohydrates) are rapidly degraded within the $Z_c^{CH_4}$, leaving mainly lipids and fatty alcohols as degradable substrates in the $Z_{p1}^{CH_4}$ for fermentation and methanogenesis.

Considering that the C_{org} represents ~20% of the dry sediment mass of the oligotrophic Lake Tantaré, i.e., that about 40% of the sediment is organic, fermentation of compounds, such as lipids, which is considered negligible in marine settings, can be a significant source of mineralized carbon in these lake sediments.

5. CONCLUSIONS

Modeling the concentrations and $\delta^{13}C$ profiles of CH_4 and DIC with reaction-transport equations reveals that OM fermenting in the sediments of a seasonally anoxic lacustrine basin is more reduced than CH_2O and yields significantly more CH_4 than DIC. We propose that the organic substrates undergoing fermentation can be represented by the general formula $C_xH_{1.87x+2z}O_z$, where z can take any value between 0 and (0.13x+2)/3. While this chemical formula is more representative of the OM fermenting in the sediments of our study site than CH_2O, its general applicability to boreal lake sediments remains to be demonstrated. If suitable for sediments deposited under other redox conditions, the current formulation of the fermenting OM in geochemical models, i.e., CH_2O, should be revised for better predictions of CH_4 cycling in boreal lakes.

The accurate fitting between the measured and modeled $\delta^{13}C$-CH_4 and $\delta^{13}C$-DIC profiles also allows quantifying in situ OM mineralization reaction rates including those of each methanogenesis pathway, and constraining the carbon isotope fractionation

factors of several OM mineralization reactions occurring under natural conditions. We conclude that nearly all of the CH_4 production in the sediments of our seasonally anoxic lacustrine basin is derived from hydrogenotrophy. A proposed explanation to rationalize the shifts in CH_4 production from acetoclastic to hydrogenotrophic methanogenesis with sediment/soil depth (Hornibrook et al., 1997; Conrad et al., 2009), as well as with variations in primary production (Wand et al., 2006; Galand et al., 2010), is that hydrogenotrophy becomes predominant when labile OM is depleted (Whiticar et al., 1986; Chasar et al., 2000; Hornibrook et al., 2000). Our observation that the predominance of the hydrogenotrophic pathway is associated with a negative COS value (−1.87) of the fermenting OM, i.e., implying that labile organic substrates such as carbohydrates and proteins are depleted, is a strong support for this interpretation. In the seasonally anoxic basin of our oligotrophic lake, the labile fraction of OM is rapidly degraded near the SWI, leaving only reduced organic compounds, i.e., lipids and fatty alcohols, to sustain hydrogenotrophy deeper in the sediments. Given the low rates of primary production in most boreal lakes and the terrigenous origin of their OM, it would not be surprising, as suggested by Hornibrook et al. (2000), that hydrogenotrophy dominates CH_4 production in the sediments of these lakes.

Acknowledgements

We thank L. Rancourt, P. Girard, J.-F. Dutil, S. Duval, A. Royer-Lavallée, A. Laberge and A. Barber for laboratory and field work assistance, and three anonymous reviewers whose comments contributed to significantly improve this manuscript. We are thankful to J.-F. Hélie, from the Laboratoire de géochimie des isotopes stables légers (UQÀM), who graciously calibrated our $\delta^{13}C$ internal standard. This work was supported

by grants to C.G., A.T. and Y.G. from the Natural Sciences and Engineering Research Council of Canada and the Fonds de Recherche Québécois – Nature et Technologies. Permission from the Québec Ministère du Développement durable, de l'Environnement et de la Lutte contre les changements climatiques to work in the Tantaré Ecological Reserve is gratefully acknowledged.

References

Alfaro-De La Torre M. C. (2001) Géochimie du cadmium dans un lac oligotrophe acide. Ph.D. thesis, INRS-EAU, Université du Québec.

Aller R. C. (2014) Sedimentary diagenesis, depositional environments, and benthic fluxes. In *Treatise on Geochemistry* (eds. Holland H. and Turekian K.) 2nd ed., Elsevier, Oxford. pp. 293-334.

Alperin M. J., Reeburgh W. S. and Whiticar M. J. (1988) Carbon and hydrogen isotope fraction resulting from anaerobic methane oxidation. *Global Biogeochem. Cycles* **2**, 279-288.

Alperin M. J., Albert D. B. and Martens C. S. (1994) Seasonal variations in production and consumption rates of dissolved organic carbon in an organic-rich coastal sediment. *Geochim. Cosmochim. Acta* **58**, 4909-4930.

Arndt S., Jørgensen B. B., LaRowe D. E., Middelburg J. J., Pancost R. D. and Regnier P. (2013) Quantifying the degradation of organic matter in marine sediments: A review and synthesis. *Earth-Sci. Rev.* **123**, 53-86.

Arning E. T., van Berk W. and Schulz H.-M. (2016) Fate and behaviour of marine organic matter during burial of anoxic sediments: Testing CH2O as generalized input parameter in reaction transport models. *Mar. Chem.* **178**, 8-21.

Baldock J. A., Masiello C. A., Gélinas Y. and Hedges J. I. (2004) Cycling and composition of organic matter in terrestrial and marine ecosystems. *Mar. Chem.* **92**, 39-64.

Barker J. F. and Fritz P. (1981) Carbon isotope fractionation during microbial methane oxidation. *Nature* **293**, 289-291.

Bastviken D., Cole J., Pace M. and Tranvik L. (2004) Methane emissions from lakes: Dependence of lake characteristics, two regional assessments, and a global estimate. *Global Biogeochem. Cycles* **18**.

Berelson W. M., Prokopenko M., Sansone F. J., Graham A. W., McManus J. and Bernhard J. M. (2005) Anaerobic diagenesis of silica and carbon in continental margin sediments: Discrete zones of TCO2 production. *Geochim. Cosmochim. Acta* **69**, 4611-4629.

Berg P., Risgaard-Petersen N. and Rysgaard S. (1998) Interpretation of measured concentration profiles in sediment pore water. *Limnol. Oceanogr.* **43**, 1500-1510.

Berner R. A. (1980) *Early Diagenesis: A Theoretical Approach*. Princeton University Press, Princeton, New Jersey.

Blair N. E. and Carter J. W. D. (1992) The carbon isotope biogeochemistry of acetate from a methanogenic marine sediment. *Geochim. Cosmochim. Acta* **56**, 1247-1258.

Borowski W. S., Paull C. K. and Ussler W. (1997) Carbon cycling within the upper methanogenic zone of continental rise sediments; An example from the methane-rich sediments overlying the Blake Ridge gas hydrate deposits. *Mar. Chem.* **57**, 299-311.

Bottinga Y. (1968) Calculation of fractionation factors for carbon and oxygen isotopic exchange in the system calcite-carbon dioxide-water. *J. Phys. Chem.* **72**, 800-808.

Bottrell S.H., Parkes R. J., Cragg B. A. and Raiswell R. (2000) Isotopic evidence for anoxic pyrite oxidation and stimulation of bacterial sulphate reduction in marine sediments. *J. Geol. Soc. (London, U. K.)* **157**, 711-714.

Boudreau B. P. (1997) *Diagenetic Models and their Implementation: Modelling Transport and Reactions in Aquatic Sediments*. 1st ed. Springer, Berlin.

Brandl H., Hanselmann K.W., Bachofen R. and Piccard J. (1993) Small-scale patchiness in the chemistry and microbiology of sediments in Lake Geneva, Switzerland. *J. Gen. Microb.* **139**, 2271-2275.

Bridgham S. D., Cadillo-Quiroz H., Keller J. K. and Zhuang Q. (2013) Methane emissions from wetlands: Biogeochemical, microbial, and modeling perspectives from local to global scales. *Glob. Chang. Biol.* **19**, 1325-1346.

Burdige D. J. (2006) *Geochemistry of Marine Sediments*. Princeton University Press, Princeton and Oxford.

Burdige D. J. (2007) Preservation of organic matter in marine sediments: Controls, mechanisms, and an imbalance in sediment organic carbon budgets? *Chem. Rev.* **107**, 467-485.

Burdige D. J. and Komada T. (2011) Anaerobic oxidation of methane and the stoichiometry of remineralization processes in continental margin sediments. *Limnol. Oceanogr.* **56**, 1781-1796.

Canavan R. W., Slomp C. P., Jourabchi P., Van Cappellen P., Laverman A.M. and van den Berg G.A. (2006) Organic matter mineralization in sediment of a coastal freshwater lake and response to salinization. *Geochim. Cosmochim. Acta* **70**, 2836-2855.

Canuel E. A. and Martens C. S. (1996) Reactivity of recently deposited organic matter: Degradation of lipid compounds near the sediment-water interface. *Geochim. Cosmochim. Acta* **60**, 1793-1806.

Carignan R., Rapin F. and Tessier A. (1985) Sediment porewater sampling for metal analysis–a comparison of techniques. *Geochim. Cosmochim. Acta* **49**, 2493-2497.

Chanton J. P. (2005) The effect of gas transport on the isotope signature of methane in wetlands. *Org. Geochem.* **36**, 753-768.

Chanton J. P., Fields D. and Hines M. E. (2006) Controls on the hydrogen isotopic composition of biogenic methane from high-latitude terrestrial wetlands. *J. Geophys. Res.: Biogeosci.* **111**.

Chappaz A., Gobeil C. and Tessier A. (2008) Geochemical and anthropogenic enrichments of Mo in sediments from perennially oxic and seasonally anoxic lakes in Eastern Canada. *Geochim. Cosmochim. Acta* **72**, 170-184.

Chasar L. S., Chanton J. P., Glaser P. H. and Siegel D. I. (2000) Methane concentration and stable isotope distribution as evidence of rhizospheric processes: Comparison of a fen and bog in the Glacial Lake Agassiz Peatland complex. *Annals of Botany* **86**, 655-663.

Clayer F., Gobeil C. and Tessier A. (2016) Rates and pathways of sedimentary organic matter mineralization in two basins of a boreal lake: Emphasis on methanogenesis and methanotrophy. *Limnol. Oceanogr.*

Conrad R. (1999) Contribution of hydrogen to methane production and control of hydrogen concentrations in methanogenic soils and sediments. *FEMS Microbiol. Ecol.* **28**, 193-202.

Conrad R. (2005) Quantification of methanogenic pathways using stable carbon isotopic signatures: a review and a proposal. *Org. Geochem.* **36**, 739-752.

Conrad R., Claus P. and Casper P. (2009) Characterization of stable isotope fractionation during methane production in the sediment of a eutrophic lake, Lake Dagow, Germany. *Limnol. Oceanogr.* **54**, 457-471.

Conrad R., Claus P. and Casper P. (2010) Stable isotope fractionation during the methanogenic degradation of organic matter in the sediment of an acidic bog lake, Lake Grosse Fuchskuhle. *Limnol. Oceanogr.* **55**, 1932-1942.

Conrad R., Klose M., Yuan Q., Lu Y. and Chidthaisong A. (2012) Stable carbon isotope fractionation, carbon flux partitioning and priming effects in anoxic soils during methanogenic degradation of straw and soil organic matter. *Soil Biol. Biochem.* **49**, 193-199.

Conrad R., Claus P., Chidthaisong A., Lu Y., Fernandez Scavino A., Liu Y., Angel R., Galand P. E., Casper P., Guerin F. and Enrich-Prast A. (2014) Stable carbon isotope biogeochemistry of propionate and acetate in methanogenic soils and lake sediments. *Org. Geochem.* **73**, 1-7.

Corbett J. E., Tfaily M. M., Burdige D. J., Glaser P. H. and Chanton J. P. (2015) The relative importance of methanogenesis in the decomposition of organic matter in northern peatlands. *J. Geophys. Res.: Biogeosci.* **120**, 280-293.

Corbett J. E., Tfaily M. M., Burdige D. J., Cooper W. T., Glaser P. H. and Chanton J. P. (2013) Partitioning pathways of CO_2 production in peatlands with stable carbon isotopes. *Biogeochemistry* **114**, 327-340.

Couture R. M., Gobeil C. and Tessier A. (2008) Chronology of atmospheric deposition of arsenic inferred from reconstructed sedimentary records. *Environ. Sci. Technol.* **42**, 6508-6513.

Couture R.-M., Fischer R., Van Cappellen R. and Gobeil C. (2016) Non-steady state diagenesis of organic and inorganic sulfur in lake sediments. *Geochim. Cosmochim. Acta* **194**, 15-33.

Cranwell P.A. (1981) Diagenesis of free and bound lipids in terrestrial detritus deposited in a lacustrine sediment. *Org. Geochem.* **3**, 79-89.

Downing J. A. and Rath L. C. (1988) Spatial patchiness in the lacustrine sedimentary environment. *Limnol. Oceanogr.* **33**, 447-458.

Duan Z. and Mao S. (2006) A thermodynamic model for calculating methane solubility, density and gas phase composition of methane-bearing aqueous fluids from 273 to 523K and from 1 to 2000bar. *Geochim. Cosmochim. Acta* **70**, 3369-3386.

Emrich K., Ehhalt D. H. and Vogel J. C. (1970) Carbon isotope fractionation during the precipitation of calcium carbonate. *Earth Planet. Sci. Lett.* **8**, 363-371.

Farrington J. W., Henrichs S. M. and Anderson R. (1977) Fatty wids and Pb210 geochronology of a sediment core from Buzzards Bay, Massachusetts. *Geochim. Cosmochim. Acta* **41**, 289-296.

Faure G. (1998) *Principles and Applications of Geochemistry.* 2nd ed., Prentice Hall.

Fey A., Claus P. and Conrad R. (2004) Temporal change of 13C-isotope signatures and methanogenic pathways in rice field soil incubated anoxically at different temperatures. *Geochim. Cosmochim. Acta* **68**, 293-306.

Galand P. E., Yrjälä K. and Conrad R. (2010) Stable carbon isotope fractionation during methanogenesis in three boreal peatland ecosystems. *Biogeosciences* **7**, 3893-3900.

Gelwicks J. T., Risatti J. B. and Hayes J. M. (1994) Carbon Isotope Effects Associated with Aceticlastic Methanogenesis. *Appl. Environ. Microbiol.* **60**, 467-472.

Happell J. D., Chanton J. P. and Showers W. J. (1995) Methane transfer across the water-air interface in stagnant wooded swamps of Florida: Evaluation of mass-transfer coefficients and isotopic fractionation. *Limnol. Oceanogr.* **40**, 290-298.

Hare L., Carignan R. and Huerta-Diaz M. A. (1994) A field study of metal toxicity and accumulation by benthic invertebrates; Implications for the acid-volatile sulfide (AVS) model. *Limnol. Oceanogr.* **39**, 1653-1668.

Harvey H. R. and Macko S. A. (1997) Kinetics of phytoplankton decay during simulated sedimentation: Changes in lipids under oxic and anoxic conditions. *Org. Geochem.* **27**, 129-140.

Hayduk W. and Laudie H. (1974) Prediction of diffusion coefficients for nonelectrolytes in dilute aqueous solutions. *AlChE J.* **20**, 611-615.

Hedges J. I. and Oades J. M. (1997) Comparative organic geochemistries of soils and marine sediments. *Org. Geochem.* **27**, 319-361.

Hedges J. I., Baldock J. A., Gelinas Y., Lee C., Peterson M. L. and Wakeham S. G. (2002) The biochemical and elemental compositions of marine plankton: A NMR perspective. *Mar. Chem.* **78**, 47-63.

Hélie J.-F. (2004) Géochimie et flux de carbone organique et inorganique dans les milieux aquatiques de l'est du Canada : exemples du Saint-Laurent et du réservoir Robert-Bourassa -approche isotopique -. Ph.D. thesis, Université du Québec à Montréal.

Hesslein R. H. (1976) Insitu sampler for close interval pore water studies. *Limnol. Oceanogr.* **21**, 912-914.

Holmkvist L., Ferdelman T. G. and Jørgensen B. B. (2011a) A cryptic sulfur cycle driven by iron in the methane zone of marine sediment (Aarhus Bay, Denmark). *Geochim. Cosmochim. Acta* **75**, 3581-3599.

Holmkvist L., Kamyshny A., Vogt C., Vamvakopoulos K., Ferdelman T. G. and Jørgensen B. B. (2011b) Sulfate reduction below the sulfate–methane transition in Black Sea sediments. *Deep-Sea Res. Pt I* **58**, 493-504.

Hornibrook E. R. C., Longstaffe F. J. and Fyfe W. S. (1997) Spatial distribution of microbial methane production pathways in temperate zone wetland soils: Stable carbon and hydrogen isotope evidence. *Geochim. Cosmochim. Acta* **61**, 745-753.

Hornibrook E. R. C., Longstaffe F. J. and Fyfe W. S. (2000) Evolution of stable carbon isotope compositions for methane and carbon dioxide in freshwater wetlands and other anaerobic environments. *Geochim. Cosmochim. Acta* **64**, 1013-1027.

IPCC (2013) Climate change 2013 : the physical science basis. In *Contribution of Working Group I to the Fifth Assessment Report of the Intergovernmental Panel on Climate Change*. (eds. Stocker T. F., Qin D., Plattner G.-K., Tignor M., Allen S. K., Boschung J., Nauels A., Xia Y., Bex V. and Midgley P. M.). Cambridge University Press, Cambridge, UK, and New York, USA.

Jähne B., Heinz G. and Dietrich W. (1987) Measurement of the diffusion coefficients of sparingly soluble gases in water. *J. Geophys. Res.* **92**, 10767-10776.

Jørgensen B. B. and Parkes R. J. (2010) Role of sulfate reduction and methane production by organic carbon degradation in eutrophic fjord sediments (Limfjorden, Denmark). *Limnol. Oceanogr.* **55**, 1338-1352.

Joshani A. (2015) Investigating organic matter preservation through complexation with iron oxides in Lake Tantaré. M.Sc. thesis, Concordia University.

Kawamura K., Ishiwatari R. and Yamakazi M. (1980) Identification of polyunsaturated fatty acids in surface lacustrine sediments. *Chem. Geol.* **28**, 31-39.

Kroll J. H., Donahue N. M., Jimenez J. L., Kessler S. H., Canagaratna M. R., Wilson K. R., Altieri K. E., Mazzoleni L. R., Wozniak A. S., Bluhm H., Mysak E. R., Smith J. D., Kolb C. E. and Worsnop D. R. (2011) Carbon oxidation state as a metric for describing the chemistry of atmospheric organic aerosol. *Nature Chem.* **3**, 133-139.

Krzycki J. A., Kenealy W. R., DeNiro M. J. and Zeikus J. G. (1987) Stable Carbon Isotope Fractionation by Methanosarcina barkeri during Methanogenesis from Acetate, Methanol, or Carbon Dioxide-Hydrogen. *Appl. Environ. Microbiol.* **53**, 2597-2599.

Laforte L., Tessier A., Gobeil C. and Carignan R. (2005) Thallium diagenesis in lacustrine sediments. *Geochim. Cosmochim. Acta* **69**, 5295-5306.

Lapham L., Proctor L. and Chanton J. P. (1999) Using Respiration Rates and Stable Carbon Isotopes to Monitor the Biodegradation of Orimulsion by Marine Benthic Bacteria. *Environ. Sci. Technol.* **33**, 2035-2039.

LaRowe D. E. and Van Cappellen P. (2011) Degradation of natural organic matter: A thermodynamic analysis. *Geochim. Cosmochim. Acta* **75**, 2030-2042.

Lettmann K. A., Riedinger N., Ramlau R., Knab N., Böttcher M. E., Khalili A., Wolff J.-O. and Jørgensen B. B. (2012) Estimation of biogeochemical rates from concentration profiles: A novel inverse method. *Estuar. Coast. Shelf Sci.* **100**, 26-37.

Liu K., Wu L., Couture R.-M., Li W. and Van Cappellen P. (2015) Iron isotope fractionation in sediments of an oligotrophic freshwater lake. *Earth Planet. Sci. Lett.* **423**, 164-172.

Martens C. S., Albert D. B. and Alperin M. J. (1999) Stable isotope tracing of anaerobic methane oxidation in the gassy sediments of Eckernförde Bay, German Baltic Sea. *Am. J. Sci.* **299**, 589-610.

Matsuda H. (1978) Early diagenesis of fatty acids in lacustrine sediments-III. Changes in fatty acid composition in the sediments from a brackish water lake. *Geochim. Cosmochim. Acta* **42**, 1027-1034.

Matsuda H. and Koyama T. (1977) Early diagenesis of fatty acids in lacustrine sediments-I. Identification and distribution of fatty acids in recent sediment from a freshwater lake. *Geochim. Cosmochim. Acta* **41**, 777-783.

Matsumoto G. I. (1989) Biogeochemical study of organic substances in Antarctic lakes. *Hydrobiologia* **172**, 265-289.

Mills J. V., Antler G. and Turchyn A. V. (2016) Geochemical evidence for cryptic sulfur cycling in salt marsh sediments. *Earth Planet. Sci. Lett.* **453**, 23-32.

Mook W. G., Bommerson J. C. and Staverman W. H. (1974) Carbon isotope fractionation between dissolved bicarbonate and gaseous carbon dioxide. *Earth Planet. Sci. Lett.* **22**, 167-176.

Nisbet E. G., Duglokencky E. J. and Bousquet P. (2014) Methane on the rise—Again. *Science* **343**, 493-495.

O'Leary M. H. (1984) Measurement of the isotope fractionation associated with diffusion of carbon dioxide in aqueous solution. *J. Phys. Chem.* **88**, 823-825.

Oelkers E. H. (1991) Calculation of diffusion coefficients for aqueous organic species at temperatures from 0 to 350°C. *Geochim. Cosmochim. Acta* **55**, 3515-3529.

Paraska D. W., Hipsey M. R. and Salmon S. U. (2014) Sediment diagenesis models: Review of approaches, challenges and opportunities. *Environ. Modell. Softw.* **61**, 297-325.

Pohlman J. W., Ruppel C., Hutchinson D. R., Downer R. and Coffin R. B. (2008) Assessing sulfate reduction and methane cycling in a high salinity pore water system in the northern Gulf of Mexico. *Mar. and Petrol. Geol.* **25**, 942-951.

Rees C. E. (1973) A steady-state model for sulphur isotope fractionation in bacterial reduction processes. *Geochim. Cosmochim. Acta* **37**, 1141-1162.

Richet P., Bottinga Y. and Javoy M. (1977) A Review of Hydrogen, Carbon, Nitrogen, Oxygen, Sulphur, and Chlorine Stable Isotope Fractionation Among Gaseous Molecules. *Annu. Rev. Earth Planet. Sci.* **5**, 65-110.

Saunois M., Bousquet P., Poulter B., Peregon A., Ciais P., Canadell J. G., Dlugokencky E. J., Etiope G., Bastviken D., Houweling S., Janssens-Maenhout G., Tubiello F. N., Castaldi S., Jackson R. B., Alexe M., Arora V. K., Beerling D. J., Bergamaschi P., Blake D. R., Brailsford G., Brovkin V., Bruhwiler L., Crevoisier C., Crill P., Covey K., Curry C., Frankenberg C., Gedney N., Höglund-Isaksson L., Ishizawa M., Ito A., Joos F., Kim H.-S., Kleinen T., Krummel P., Lamarque J.-F., Langenfelds R., Locatelli R., Machida T., Maksyutov S., McDonald K. C., Marshall J., Melton J. R., Morino I., Naik V., amp, apos, Doherty S., Parmentier F.-J. W., Patra P. K., Peng C., Peng S., Peters G. P., Pison I., Prigent C., Prinn R., Ramonet M., Riley W. J., Saito M., Santini M., Schroeder R., Simpson I. J., Spahni R., Steele P., Takizawa A., Thornton B. F., Tian H., Tohjima Y., Viovy N., Voulgarakis A., van Weele M., van der Werf G. R., Weiss R., Wiedinmyer C., Wilton D. J., Wiltshire A., Worthy D., Wunch D., Xu X., Yoshida Y., Zhang B., Zhang Z. and Zhu Q. (2016) The global methane budget 2000–2012. *Earth Syst. Sci. Data* **8**, 697-751.

Shindell D. T., Faluvegi G., Koch D. M., Schmidt G. A., Linger N. and Bauer S. E. (2009) Improved attribution of climate forcing to emissions. *Science* **326**, 716-718.

Stumm W. and Morgan J. J. (1996) Aquatic Chemistry. 3rd ed. Wiley.

Timsic S. and Patterson W. P. (2014) Spatial variability in stable isotope values of surface waters of Eastern Canada and New England. *Journal of Hydrology* **511**, 594-604.

Tipping E. (2002) Cation Binding by Humic Substances. Cambridge Univ. Press.

Tissot B. P. and Welte D. H. (1984) *Petroleum Formation and Occurrence*. 2nd ed. Springer, Berlin.

Tranvik L. J., Downing J. A., Cotner J. B., Loiselle S. A., Striegl R. G., Ballatore T. J., Dillon P., Finlay K., Fortino K., Knoll L. B., Kortelainen P. L., Kutser T., Larsen S., Laurion I., Leech D. M., McCallister S. L., McKnight D. M., Melack J. M., Overholt E., Porter J. A., Prairie Y., Renwick W. H., Roland F., Sherman B. S.,

Schindler D. W., Sobek S., Tremblay A., Vanni M. J., Verschoor A. M., von Wachenfeldt E. and Weyhenmeyer G. A. (2009) Lakes and reservoirs as regulators of carbon cycling and climate. *Limnol. Oceanogr.* **54**, 2298-2314.

Treude T., Krause S., Maltby J., Dale A. W., Coffin R. and Hamdan L. J. (2014) Sulfate reduction and methane oxidation activity below the sulfate-methane transition zone in Alaskan Beaufort Sea continental margin sediments: Implications for deep sulfur cycling. *Geochim. Cosmochim. Acta* **144**, 217-237.

Ullman W. J. and Aller R. C. (1982) Diffusion-coefficients in nearshore marine-sediments. *Limnol. Oceanogr.* **27**, 552-556.

Van Cappellen P. and Wang Y. F. (1996) Cycling of iron and manganese in surface sediments: A general theory for the coupled transport and reaction of carbon, oxygen, nitrogen, sulfur, iron, and manganese. *Am. J. Sci.* **296**, 197-243.

Verpoorter C., Kutser T., Seekell D. A. and Tranvik L. J. (2014) A global inventory of lakes based on high-resolution satellite imagery. *Geophys. Res. Lett.* **41**, 6396-6402.

Wand U., Samarkin V. A., Nitzsche H. M. and Hubberten H. W. (2006) Biogeochemistry of methane in the permanently ice-covered Lake Untersee, central Dronning Maud Land, East Antarctica. *Limnol. Oceanogr.* **51**, 1180-1194.

Werth M. and Kuzyakov Y. (2010) ^{13}C fractionation at the root–microorganisms–soil interface: A review and outlook for partitioning studies. *Soil Biol. Biochem.* **42**, 1372-1384.

Westrich J. T. and Berner R. A. (1984) The role of sedimentary organic matter in bacterial sulfate reduction: The G model tested. *Limnol. Oceanogr.* **29**, 236-249.

Whiticar M. J. (1999) Carbon and hydrogen isotope systematics of bacterial formation and oxidation of methane. *Chem. Geol.* **161**, 291-314.

Whiticar M. J. and Faber E. (1986) Methane oxidation in sediment and water column environments—Isotope evidence. *Org. Geochem.* **10**, 759-768.

Whiticar M. J., Faber E. and Schoell M. (1986) Biogenic methane formation in marine and fresh-water environments: CO_2 reduction *vs.* acetate fermentation—Isotope evidence. *Geochim. Cosmochim. Acta* **50**, 693-709.

Wilke C. R. and Chang P. (1955) Correlation of diffusion coefficients in dilute solutions. *AlChE J.* **1**, 264-270.

Zeebe R. E. (2011) On the molecular diffusion coefficients of dissolved CO_2, HCO_3^- and CO_3^{2-} and their dependence on isotopic mass. *Geochim. Cosmochim. Acta* **75**, 2483-2498.

Table 1: Main reactions (r_1–r_6) considered in sediment OM mineralization along with their reaction rates (R_1–R_6) and carbon isotopic fractionation factors (α_1–α_6)

Description	**Reaction**	**ID**
CO_2 production due to OM fermentation [a]		
	$C_xH_yO_z + (x+\nu-z)H_2O \xrightarrow[\alpha_1]{R_1} \left(\frac{x-\nu}{2}\right)CH_3COOH + \nu CO_2 + \left(\frac{y}{2}-z+2\nu\right)H_2$	r_1
Methanogenesis via		
Acetate fermentation	$CH_3COOH \xrightarrow[\alpha_2]{R_2} CH_4 + CO_2$	r_2
hydrogenotrophy	$CO_2 + 4H_2 \xrightarrow[\alpha_3]{R_3} CH_4 + 2H_2O$	r_3
CO_2 production due to		
methanotrophy	$CH_4 + \text{Oxidant} \xrightarrow[\alpha_4]{R_4} CO_2 + \text{Reducer}$	r_4
OM oxidation	$OM + \text{Oxidant} \xrightarrow[\alpha_5]{R_5} CO_2 + \text{Reducer}$	r_5
Precipitation of siderite	$Fe^{2+} + CO_3^{2-} \xrightarrow[\alpha_6]{R_6} FeCO_{3(s)}$	r_6

[a] where ν can have any value between 0 and x.

Table 2: Net reaction rates (fmol cm^{-3} s^{-1}) of CH_4 ($R_{net}^{CH_4}$) and DIC (R_{net}^{DIC}) as well as rates (R_1–R_6) of reactions involved in OM mineralization in each zone according to scenarios S1 and S2.

Zones	$R_{net}^{CH_4}$	R_{net}^{DIC}	R_i	
			S1	S2
$Z_c^{CH_4}$	−23	114	$R_1 = 0$ $R_2 = 0$ $R_3 = 0$ $R_4 = 23$ $R_5 = 125$ $R_6 = -34$	$R_1 = 0$ $R_2 = 0$ $R_3 = 0$ $R_4 = 23$ $R_5 = 125$ $R_6 = -34$
$Z_{p1}^{CH_4}$	116	42	$R_1 = 158$ $R_2 = 0$ $R_3 = 116$ $R_4 = 0$ $R_5 = 0$ $R_6 = 0$	$R_1 = 0$ $R_2 = 79$ $R_3 = 37$ $R_4 = 0$ $R_5 = 0$ $R_6 = 0$
$Z_{p2}^{CH_4}$	11	−13	$R_1 = 0$ $R_2 = 0$ $R_3 = 12$ $R_4 = 0$ $R_5 = 0$ $R_6 = 0$	$R_1 = 0$ $R_2 = 0$ $R_3 = 12$ $R_4 = 0$ $R_5 = 0$ $R_6 = 0$

Table 3: Values of the isotopic fractionation factors (α) and molecular diffusivity ratios (f) used as input parameters in Eq. 9.

Parameters	Range	References	Default	Retained in this study
f–DIC	1.000–1.001	a,b	1.000	1.000
f–CH_4	1.000–1.003	c	1.000	1.003
α_1 and α_5		d,e,f	1.000	1.000
α_2-CH_4	1.021–1.027	g,h	1.024	
α_2-CO_2	1.021–1.027	h	1.024	
α_3	1.050–1.095	i,j	1.075	1.081
α_4	1.005–1.031	k,l	1.005	1.016
α_6	0.990–0.998	m,n	0.996	0.996

References: (a) O'Leary 1984, (b) Jähne et al. 1987, (c) Chanton 2005, (d) Lapham et al. 1999, (e) Werth and Kuzyakov 2010, (f) Conrad et al. 2012, (g) Krzycki et al. 1987, (h) Gelwicks et al. 1994, (i) Whiticar 1999, (j) Conrad et al. 2014, (k) Barker and Fritz 1981, (l) Alperin et al. 1988, (m) Bottinga 1968 and (n) Emrich et al. (1970).

Table 4: Influence of the average carbon oxidation state (COS) of organic substrates on fermentation products

Compounds	Formula	COS	CH_4/CO_2 production ratio assuming complete fermentation	Reference
Glycolic acid	$C_2H_4O_3$	+1.00	0.60	LaRowe and Van Cappellen 2011
Glucose	$C_6H_{12}O_6$	0.00	1.00	Corbett et al. 2015
C_{16}-fatty acid	$C_{16}H_{32}O_2$	−1.75	2.56	Arning et al. 2016
C_{16}-fatty alcohol	$C_{16}H_{34}O$	−2.00	3.00	Arning et al. 2016

Figure captions

Figure 1: Replicate porewater profiles of CH_4 (a, b and c), $\delta^{13}C\text{-}CH_4$ (d), DIC (e), $\delta^{13}C$-DIC (f), SO_4^{2-} (g), ΣS(−II) (h) and Fe (i). Different symbols indicate data from different peepers and empty symbols are for concentrations below detection limit. The horizontal dotted lines indicate the sediment-water interface.

Figure 2: Comparison of modeled (red line) and average (n = 3) measured (empty symbols) concentrations and $\delta^{13}C$ profiles of CH_4 (a and c) and DIC (b and d). The horizontal dotted line indicates the sediment–water interface and the thick blue line (panels a and b) represents the net solute reaction rate (R_{net}^{solute}). The blue and red colored areas correspond to production and consumption zones, respectively.

Figure 3: $\delta^{13}CO_2$ versus $\delta^{13}C\text{-}CH_4$ graph showing the hydrogenotrophic (blue), acetoclastic (red) and CH_4 oxidation (green) domains (modified from Whiticar 1999) along with our measured data (empty symbols). The circles and squares indicate datapoints above and below the sediment–water interface, respectively.

Figure 4: Comparison of the simulated (lines) and measured average (n = 3) $\delta^{13}C$ profiles of CH_4 (empty squares) and DIC (empty circles). The red and blue continuous lines are the profiles simulated with default values for scenarios S1 and S2, respectively. The horizontal dotted line indicates the sediment–water interface.

Figure 5: Norm of residuals (N_{res}), calculated with Eq. 10, for the $\delta^{13}C$-DIC (blue line) and the $\delta^{13}C\text{-}CH_4$ (red line) profiles as a function of α_3 (a) or as a function of the proportion of CH_4 produced through acetate fermentation (b). The black line is the sum of the N_{res} values for the $\delta^{13}C\text{-}CH_4$ and the $\delta^{13}C$-DIC profiles, and the vertical dotted blue and dashed red lines indicate the minimum N_{res} value for the $\delta^{13}C$-DIC and

δ^{13}C-CH_4 profiles, respectively. The modelled profiles of δ^{13}C-DIC and δ^{13}C-CH_4 were obtained with default parameter values, except α_3 values, for scenario S1 in panel a and with optimized parameter values in panel b.

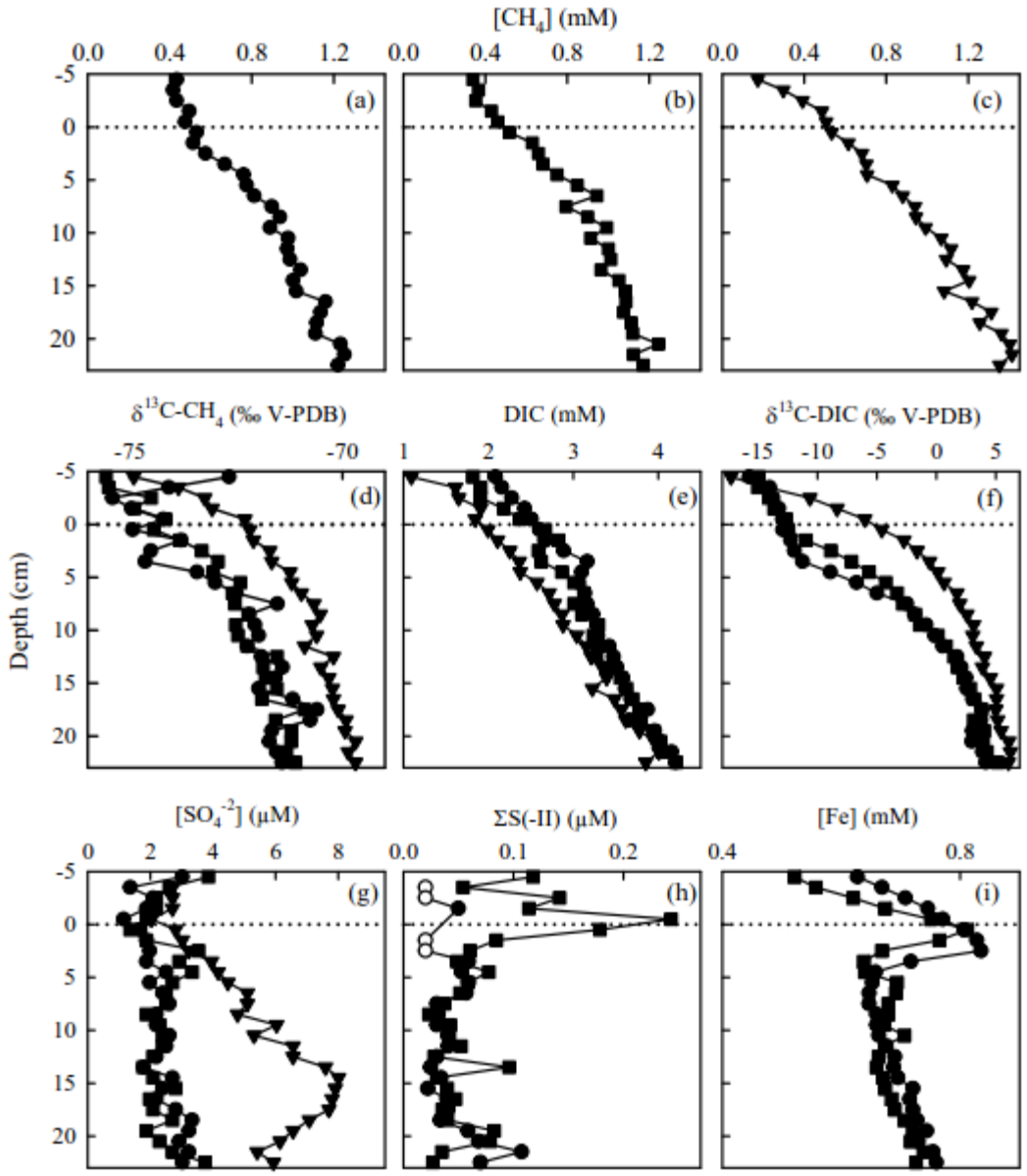
[CH4] (mM)
0.0 0.4 0.8 1.2
(a)
(b)
(c)
δ13C-CH4 (‰ V-PDB)
-75 -70
DIC (mM)
1 2 3 4
δ13C-DIC (‰ V-PDB)
-15 -10 -5 0 5
(d)
(e)
(f)
Depth (cm)
[SO4-2] (µM)
0 2 4 6 8
ΣS(-II) (µM)
0.0 0.1 0.2
[Fe] (mM)
0.4 0.8
(g)
(h)
(i)
-5 0 5 10 15 20

Figure 1

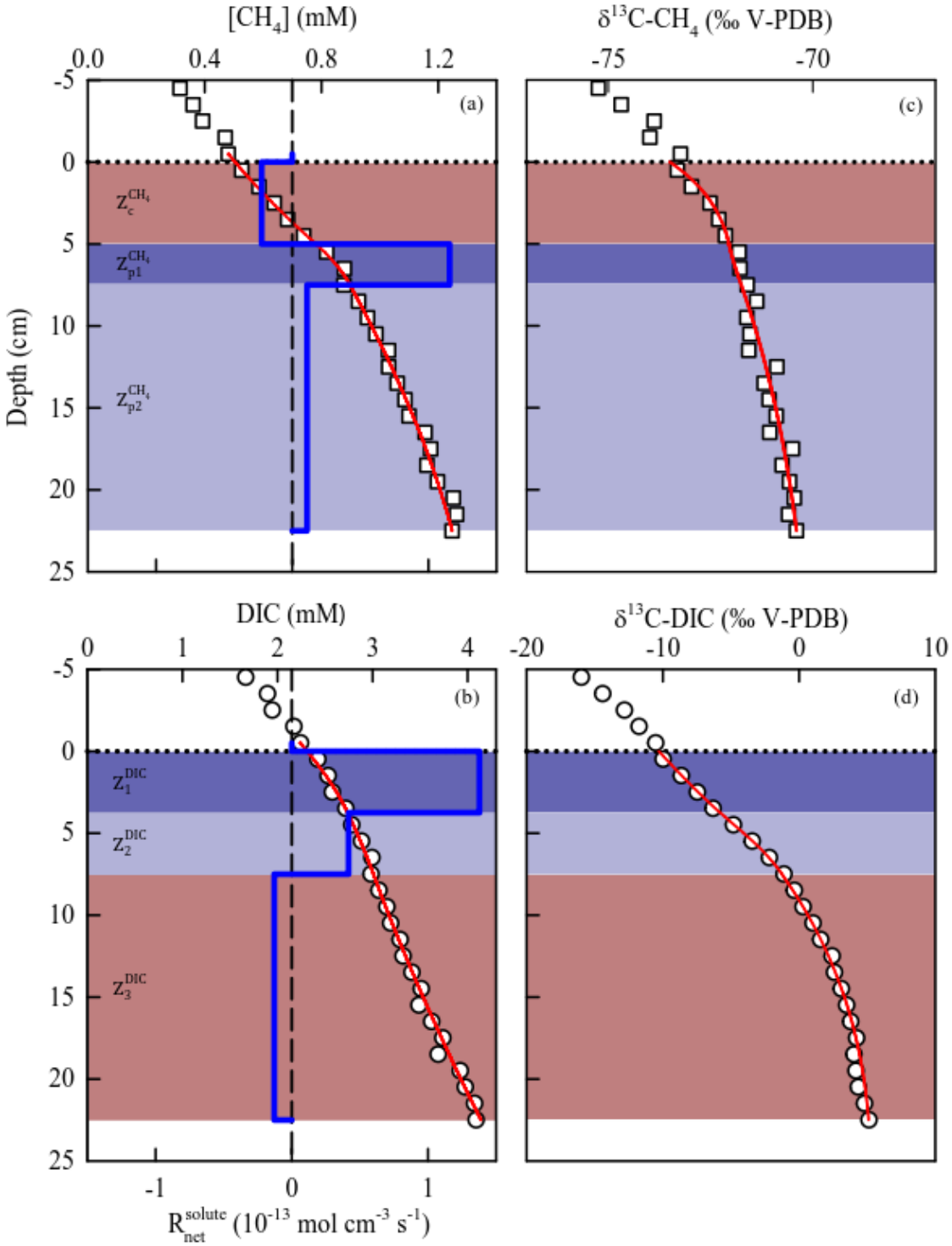
[CH4] (mM)
δ13C-CH4 (‰ V-PDB)
DIC (mM)
δ13C-DIC (‰ V-PDB)
Depth (cm)
(a)
(b)
(c)
(d)
Rnet solute (10-13 mol cm-3 s-1)

Figure 2

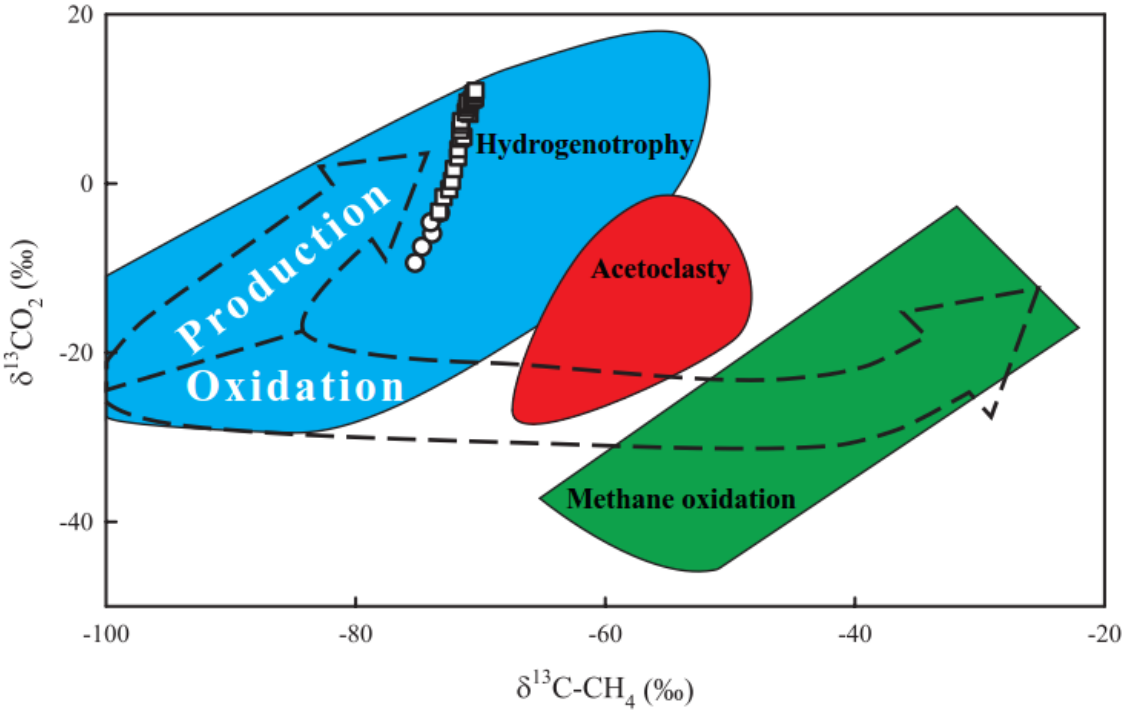

Figure 3

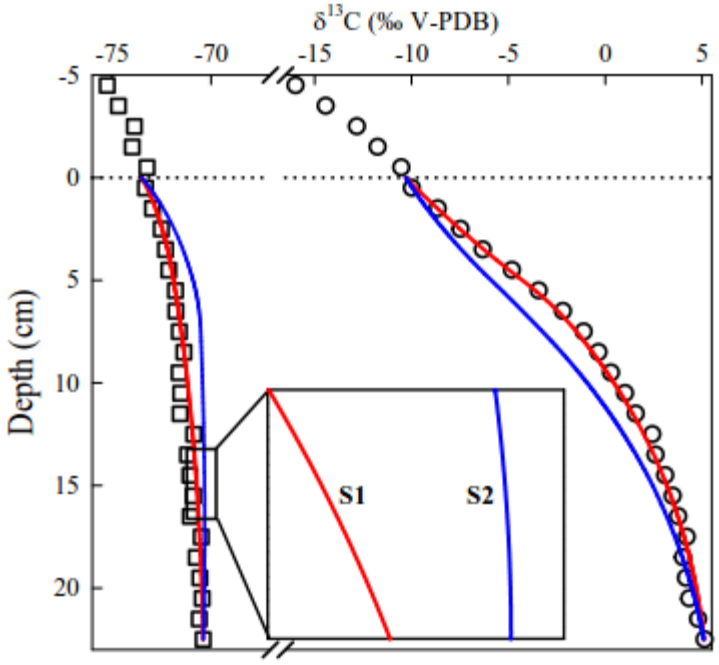

Figure 4

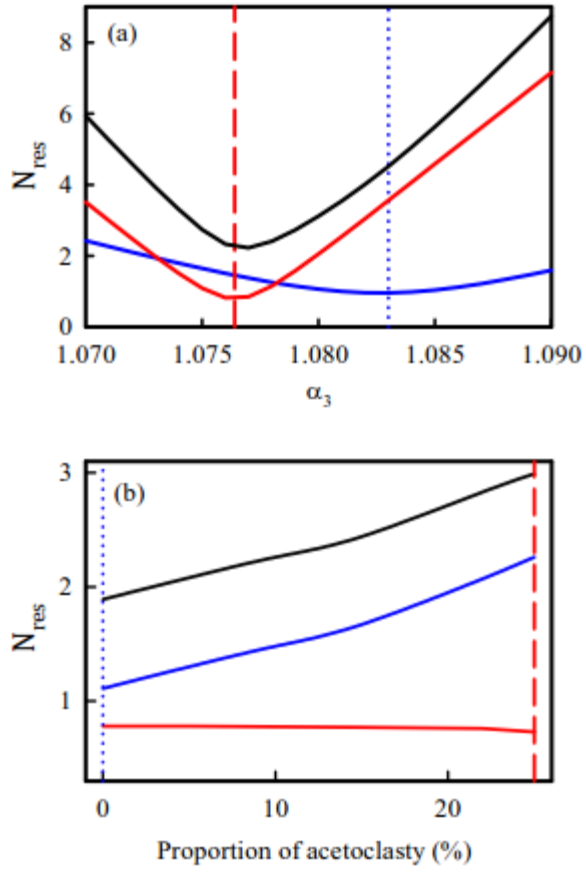

Figure 5